Title

Shaking Table Test of a Half-Scale Geosynthetic-Reinforced Soil Bridge Abutment

Journal

Geotechnical Testing Journal, 41(1)

ISSN

0149-6115

Authors

Zheng, Yewei
Sander, Andrew C
Rong, Wenyong
et al.

Publication Date

2018

DOI

10.1520/gtj20160268

Peer reviewed

Shaking Table Test of a Half-Scale Geosynthetic-Reinforced Soil Bridge Abutment

Journal:	*Geotechnical Testing Journal*
Manuscript ID	GTJ-2016-0268.R2
Manuscript Type:	Technical Manuscript
Date Submitted by the Author:	n/a
Complete List of Authors:	Zheng, Yewei; University of California San Diego, Department of Structural Engineering Sander, Andrew; University of California San Diego, Department of Structural Engineering Rong, Wenyong; University of California San Diego, Department of Structural Engineering Fox, Patrick; The Pennsylvania State University, Civil and Environmental Engineering Shing, Benson; University of California San Diego, Department of Structural Engineering McCartney, John; University of California San Diego, Department of Structural Engineering
ASTM Committees and Subcommittees:	D35.01 Mechanical Properties < D35 Committee on Geosynthetics
Keywords:	Shaking table testing, reduced-scale physical model, geosynthetic-reinforced soil, bridge abutment, geogrid
Abstract:	This paper presents an experimental study of the dynamic response of a half-scale geosynthetic-reinforced soil (GRS) bridge abutment system using a shaking table. Experimental design of the model specimen followed established similitude relationships for shaking table tests of reduced-scale models in a 1g gravitational field, including scaling of model geometry, geosynthetic reinforcement stiffness, backfill soil modulus, bridge load, and characteristics of the earthquake motions. The 2.7 m-high GRS bridge abutment was constructed using well-graded sand backfill, modular facing blocks, and uniaxial geogrid reinforcement with a vertical spacing of 0.15 m in both the longitudinal and transverse directions. A bridge beam was placed on the GRS bridge abutment at one end and on a concrete support wall resting on a sliding platform off the shaking table at the other end. The GRS bridge abutment system was subjected to a series of input motions in the longitudinal direction. Results indicate that the testing system performed well, and that the GRS bridge abutment experienced small deformations. For two earthquake motions, the maximum incremental residual facing displacement in model scale was 1.0 mm, and the average incremental residual bridge seat settlement in model scale was 1.4 mm, which corresponds to a vertical strain of 0.7%.

Shaking Table Test of a Half-Scale Geosynthetic-Reinforced Soil Bridge Abutment

Yewei Zheng[1], Andrew C. Sander[2], Wenyong Rong[3], Patrick J. Fox[4], P. Benson Shing[5], and John S. McCartney[6]

ABSTRACT

This paper presents an experimental study of the dynamic response of a half-scale geosynthetic-reinforced soil (GRS) bridge abutment system using a shaking table. Experimental design of the model specimen followed established similitude relationships for shaking table tests of reduced-scale models in a 1*g* gravitational field, including scaling of model geometry, geosynthetic reinforcement stiffness, backfill soil modulus, bridge load, and characteristics of the earthquake motions. The 2.7 m-high GRS bridge abutment was constructed using well-graded sand backfill, modular facing blocks, and uniaxial geogrid reinforcement with a vertical spacing of 0.15 m in both the longitudinal and transverse directions. A bridge beam was placed on the GRS bridge abutment at one end and on a concrete support wall resting on a sliding platform off the shaking table at the other end. The GRS bridge abutment system was subjected to a series of input motions in the longitudinal direction. Results indicate that the testing system performed well, and that the GRS bridge abutment experienced small deformations. For two earthquake motions, the maximum incremental residual facing displacement in model scale was 1.0 mm, and the average incremental residual bridge seat settlement in model scale was 1.4 mm, which corresponds to a vertical strain of 0.7%.

Keywords

Shaking table test, reduced-scale model, geogrid, geosynthetic-reinforced soil, bridge abutment

[1] Ph.D. Candidate, Department of Structural Engineering, University of California, San Diego, La Jolla, CA, 92093-0085; email: y7zheng@ucsd.edu

[2] Ph.D. Candidate, Department of Structural Engineering, University of California, San Diego, La Jolla, CA, 92093-0085; email: asander@eng.ucsd.edu

[3] Graduate Research Assistant, Department of Structural Engineering, University of California, San Diego, La Jolla, CA, 92093-0085; email: w1rong@eng.ucsd.edu

[4] Shaw Professor and Head, Ph.D., P.E., Department of Civil and Environmental Engineering, Pennsylvania State University, University Park, PA 16802; email: pjfox@engr.psu.edu

[5] Professor and Chair, Ph.D., Department of Structural Engineering, University of California, San Diego, La Jolla, CA, 92093-0085; email: pshing@ucsd.edu

[6] (corresponding author) Associate Professor, Ph.D., P.E., Department of Structural Engineering, University of California, San Diego, La Jolla, CA, 92093-0085; email: mccartney@ucsd.edu

INTRODUCTION

Physical model testing is an important method to investigate the dynamic response of reinforced soil structures, such as slopes, retaining walls and bridge abutments. Such tests are typically performed using large-scale shaking tables in the laboratory or small-scale shaking tables mounted on a geotechnical centrifuge. Although some shaking tables are sufficiently large to accommodate full-scale reinforced soil structures with the actual materials and construction techniques used in the field (Ling et al. 2005, 2009, 2012; Fox et al. 2015), the significant time and cost involved with such tests generally preclude parametric evaluations. Geotechnical centrifuge testing, on the other hand, uses much smaller physical models and permits general parametric studies under realistic stress conditions; however, the materials and soil preparation techniques often differ from those used in practice (Casey et al. 1991; Sakaguchi 1996; Howard et al. 1998; Nova-Roessig and Sitar 2006; Siddharthan et al. 2004; Liu et al. 2010). An alternative approach is to perform tests on reduced-scale models using large 1*g* shaking tables in the laboratory; however, this requires special considerations of similitude relationships to ensure that the stress-strain response is similar to the full-scale prototype structure.

Geosynthetic-reinforced soil (GRS) bridge abutments have been widely adopted as a result of construction, performance and cost advantages over traditional pile-support designs, and significant experimental and numerical modeling research has been conducted for static loading conditions (Wu et al. 2001, 2006; Helwany et al. 2007; Nicks et al. 2013, 2016; Zheng and Fox 2016, 2017). However, seismic events represent a severe loading condition and there is some reluctance to use this technology in high seismic areas without further testing and evaluation. Seismic compression of the abutment and associated bridge seat settlement is of particular concern. The shaking table tests conducted by Helwany et al. (2012) on a 3.6 m-high GRS bridge abutment indicated no significant distress for horizontal accelerations up to 1*g*. Based on the success of these tests, more investigations are warranted on the seismic response of GRS bridge abutments for various configurations and loading conditions. This paper presents the experimental design for a dynamic testing program conducted on half-scale GRS bridge abutment specimens using a large laboratory shaking table. The similitude relationships are discussed, materials and instrumentation are described, and results from a typical test are presented to highlight the testing approach and demonstrate the response of the testing system and a GRS bridge abutment specimen for different input motions.

BACKGROUND

Reduced-scale model tests provide a more economical option than tests on full-scale prototype structures and have been widely used in geotechnical engineering to investigate the behavior of complex systems. Richardson and Lee (1975) pioneered the use of 1*g* shaking table tests to investigate failure modes for 0.3 m-high soil walls reinforced with aluminum strips and subjected to sinusoidal motions. Small-scale shaking table tests also have been conducted to evaluate the dynamic response of GRS walls with various facing types (Sakaguchi 1996; Koseki et al. 1998; Matsuo et al. 1998; Latha and Krishna 2008; Krishna and Latha 2009). However, as these studies did not include scaling of model geometry or material properties, the results may be less representative of the actual response of prototype structures.

For shaking table tests on reduced-scale models in a 1*g* gravitational field, similitude relationships must be considered to produce similar response between model and prototype structures. The similitude relationships proposed by Iai (1989) have been widely used for 1*g* shaking table tests, including tests for GRS walls (El-Emam and Bathurst 2004, 2005, 2007; Guler and Enunlu 2009; Sabermahani et al. 2009; Guler and Selek 2014; Latha and Santhanakumar 2015; Panah et al. 2015). Iai (1989) hypothesized that the moduli of materials in the model should be reduced so that the reduced-scale model will have a similar stress-strain response under lower stress conditions as the prototype structure. Theoretical scaling factors for the similitude relationships are summarized in Table 1.

El-Emam and Bathurst (2004, 2005, 2007) performed fourteen shaking table tests on 1 m-high, 1/6-scale GRS walls with a full-height rigid facing panel, low stiffness geogrid (90 kN/m), and no surcharge load. The model walls were subjected to a stepped-amplitude sinusoidal motion with a predominant frequency of 5 Hz. Experimental results showed that facing displacements could be reduced by using a smaller facing panel mass, an inclined facing panel, longer reinforcement, stiffer reinforcement, and smaller vertical reinforcement spacing. Guler and Selek (2014) reported a series of reduced-scale shaking table tests on GRS walls with modular block facing and no surcharge load to investigate the effects of various factors, including peak ground acceleration (PGA), reinforcement length and spacing, model scale, and grouting of the top two courses of facing blocks. Earthquake motions also were scaled to match the Iai (1989) similitude relationships. Results indicated that accelerations were not affected by

model scale, but facing displacements for the prototype structure increased with decreasing model scale. Ling et al. (2005, 2012) reported a series of large-scale shaking table tests for 2.8 m-high GRS walls with modular block facing and no surcharge load using both sand and silty sand backfill soils. Performance was improved by increasing reinforcement length for top layers and reducing reinforcement vertical spacing. The unsaturated conditions for the silty sand backfill also improved performance. Fox et al. (2015) conducted a full-scale shaking table test on a 6.1 m-high GRS wall with modular block facing using a large soil confinement box. The confinement box had a fundamental frequency of 22 Hz, which is above the normal operating frequency band of the shaking table. Accordingly, the box moved in phase with the table and provided a rigid boundary condition. The GRS wall experienced a permanent displacement of 56 mm at the top after the completion of the testing program, which may be attributed to the relatively large reinforcement vertical spacing of 0.6 m. The ultimate state of the GRS wall indicated moderate damage, including two significant cracks in the backfill soil with a width of more than 30 mm - one at the back of the reinforced soil zone and one near the rear boundary - but no collapse.

Helwany et al. (2012) reported the only shaking table tests on a large-scale GRS bridge abutment. The abutment model had a total height of 3.6 m, including a 3.2 m-high lower wall and 0.4 m-high upper wall, with an average applied vertical stress of 111 kPa from a concrete footing that supported individual steel bridge beams. The other ends of the bridge beams were supported on rollers. The GRS bridge abutment was reinforced using a woven polypropylene geotextile with a vertical spacing of 0.2 m. The backfill soil was poorly-graded gravel with sand and clay, and had a friction angle of 44°. The abutment model was subjected to a series of horizontal sinusoidal motions with increasing amplitude. No damage was observed until the acceleration reached 0.67*g*, and no significant distress occurred for accelerations up to 1*g*. The bridge seat experienced an incremental settlement of 50 mm when the acceleration was increased from 0.67*g* to 1*g*.

EXPERIMENTAL PROGRAM

UCSD Powell Structural Laboratory Shaking Table

The indoor shaking table at the University of California, San Diego (UCSD) Powell Structural Laboratory has dimensions of 5 m × 3 m and a maximum payload capacity of 356 kN. The table slides horizontally on two stationary shafts and is driven by a servo-hydraulic actuator with a static capacity of 490 kN, dynamic capacity of 405 kN, and maximum stroke of ± 150 mm. The shaking table was refurbished prior to this study to increase the fidelity of dynamic motion (Trautner et al. 2017).

Similitude Considerations

The Iai (1989) similitude relationships (Table 1) were used in the current study. Considering the size and payload capacity of the shaking table, a length scaling factor of $\lambda = 2$ was chosen, and is defined as the ratio of prototype length to model length. A GRS bridge abutment with a total height of 5.4 m and a typical bridge clearance height of 4.5 m was selected as the prototype structure. Therefore, a half-scale GRS bridge abutment model with a total height of 2.7 m and a clearance height of 2.25 m was constructed and tested on the shaking table. Model geometry, geosynthetic reinforcement stiffness, backfill soil modulus, bridge load, and characteristics of the earthquake motions were scaled accordingly using the factors given in Table 1.

Test Configuration

The shaking table test configuration for the bridge system in the longitudinal direction is shown in Figure 1. The bridge beam has dimensions of 6.4 m × 0.9 m × 0.45 m (length × width × height), and is placed on a bridge seat that rests on the GRS bridge abutment at one end and on a concrete support wall that rests on a sliding platform at the other end. The bottom of the concrete support wall is rigidly connected to the shaking table using steel beams and experiences the same motion as the table. The bridge beam represents a longitudinal slice of a prototype bridge superstructure whose length was selected to accommodate the available laboratory space. Elastomeric bearing pads (model NEOSORB, Voss Engineering, Inc.) with plan dimensions of 0.45 m × 0.9 m, thickness of 25 mm, and elastic modulus of 3.6 MPa were placed under both ends of the bridge beam. The seismic joint (i.e., gap) between the bridge beam and vertical back

wall of the bridge seat is 25 mm wide. During shaking, the bridge beam interacts with the GRS bridge abutment and support wall through friction developed on the bearing pads and potentially contacts (i.e., impacts) with the back wall of the bridge seat. The clear distance between the top of the wall facing and bottom of the bridge beam is 0.15 m.

The self-weight of the concrete bridge beam is 65 kN, and additional dead weights (steel plates) of 33 kN are evenly distributed and rigidly attached to the beam to produce the desired total bridge weight (98 kN) while keeping the mass center of the beam relatively low to minimize rocking. The total weight of the beam and dead weights produces an average vertical stress of 121 kPa on top of the bridge seat. The bridge seat has a self-weight of 7 kN and a bottom surface with plan dimensions of 0.65 m × 1.3 m. The average vertical stress on the backfill soil from the bridge seat is 66 kPa, which corresponds to a prototype vertical stress of 132 kPa and is in the typical range for GRS bridge abutments in the field (Adams et al. 2011).

The GRS bridge abutment has modular block facing on three sides, including a front wall facing perpendicular to the longitudinal direction and two side wall facings perpendicular to the transverse direction. The back of the GRS bridge abutment is supported by a rigid reaction wall consisting of a steel frame with plywood face. The reaction wall was designed to be sufficiently stiff to provide at-rest conditions during construction and experience minimal deflections during shaking. Although the reaction wall moves in phase with the shaking table and thus does not reproduce the deformation boundary condition of a retained soil mass in the field, this simple configuration can be readily incorporated into numerical simulations for calibration purposes. To reduce effects of the reaction wall on the abutment response, the length of the retained soil zone was maximized within the geometry and payload constraints of the table. The total weight of the entire bridge system is 450 kN.

The GRS bridge abutment model has a total height of 2.7 m, consisting of a 2.1 m-high lower GRS wall and a 0.6 m-high upper wall, resting on a 0.15 m-thick foundation soil layer placed directly on the shaking table. A top view diagram is shown in Figure 2(a) and cross-sectional view diagrams in the longitudinal and transverse directions are shown in Figures 2(b) and 2(c), respectively. The abutment has plan dimensions of 2.35 m × 2.10 m, including wall facing blocks. The bridge seat rests on top of the backfill soil for the lower GRS wall and has a setback distance of 0.15 m from each of the three wall facings. The lower GRS wall was constructed in fourteen 0.15 m-thick soil lifts. Each lift includes uniaxial reinforcement layers in

the longitudinal direction (i.e., direction of shaking), and the transverse direction. Uniaxial geogrids were selected for this study as they are commonly used in GRS bridge abutments, even though they posed a challenge due to the narrow width of the model abutment considered in this study compared to the width of typical GRS bridge abutments. The longitudinal reinforcement layers are frictionally connected to the front wall facing and extend 1.47 m into the backfill soil while the transverse reinforcement layers are frictionally connected to each side wall facing and extend 0.8 m into the backfill soil, and meet (but are not connected) at the center. The transverse reinforcement layers and side wall facing blocks are offset by 25 mm vertically from the longitudinal reinforcement layers and front wall facing blocks to avoid direct contact. Although longitudinal and transverse reinforcement layers are in close proximity vertically, the maximum particle size of the backfill soil is sufficiently small to permit typical soil-reinforcement interaction. The length of the retained soil zone between the reinforced soil zone and reaction wall is 0.63 m. Transverse reinforcement layers support the side walls in the retained soil zone and are not connected to transverse reinforcements in the reinforced soil zone.

The support wall for the other end of the bridge beam rests on a sliding platform, as shown in Figure 3. Based on the low friction boundary concept developed by Fox et al. (1997, 2006), this platform consists of 273 rolling stainless steel balls (diameter = 19 mm) sandwiched between two stainless steel plates (thickness = 6 mm). The steel balls are placed inside a plastic guide plate (thickness = 13 mm) with 273 oversized holes (diameter = 25 mm) to keep the balls orderly during shaking tests. A 13 mm-thick rubber sheet is placed between the sliding platform and the support wall to reduce stress concentrations on the sliding platform. The base of the support wall is connected to the shaking table using steel beams to transmit table motions and ensure that the entire system is shaken uniformly.

Materials

The backfill soil has the particle size gradation curve shown in Figure 4(a), coefficient of uniformity C_u = 6.1, coefficient of curvature C_z = 1.0, and is classified as well-graded sand (SW) according to the Unified Soil Classification System (USCS). Soil properties are summarized in Table 2. After application of the similitude relationships (λ = 2) in Table 1, the mean particle size D_{50} of 0.85 mm corresponds to a prototype value of 1.7 mm, which still falls within the sand-size range. The specific gravity is 2.61, and the maximum and minimum void

ratios are 0.853 and 0.371, respectively. Inspection of the standard Proctor compaction curve shown in Figure 4(b) indicates that compaction water content does not have a significant effect on dry unit weight for this sand (i.e., the curve is essentially flat).

Target soil compaction conditions for construction of the GRS bridge abutment model were gravimetric water content w_c = 5% and relative density D_r = 70%. The target relative density was selected to meet the similitude relationships and to obtain reproducible densities using a vibrating plate compactor. With regard to the similitude criterion, a series of triaxial compression tests were conducted on dry sand specimens with different relative densities and yielded a secant modulus at 0.5% axial strain for D_r = 70% and confining stress σ = 34 kPa that was approximately one-half that for D_r = 85% and σ = 69 kPa. A relative density of 85% corresponds to a relative compaction of 98% for standard Proctor effort and is within the typical range of field compaction requirements for in-service GRS bridge abutments. For D_r = 70%, the dry backfill sand has a peak friction angle ϕ'_p = 51.3° and zero cohesion.

A hanging column test was performed on a sand specimen with D_r = 70% to measure the soil water retention curve (SWRC) for both drying and wetting paths. The SWRC data was fitted using the van Genuchten (1980) model:

$$\theta = \theta_r + (\theta_{\max} - \theta_r)\left[1 + (\alpha_{vG}\psi)^{N_{vG}}\right]^{-\left(1-\frac{1}{N_{vG}}\right)} \quad (1)$$

where θ is the volumetric water content (volume of water/volume of soil), ψ is the matric suction, $\theta_{\max}$ is the volumetric water content at zero matric suction for either path, θ_r is the residual saturation, and α_{vG} and N_{vG} are the van Genuchten (1980) SWRC model parameters.

The geosynthetic reinforcement is a uniaxial high density polyethylene (HDPE) geogrid (Tensar LH800). Tensile tests on single rib specimens were conducted in the laboratory according to ASTM D6637 (2015). For a strain rate of 10%/min, the geogrid has a secant stiffness at 5% strain $J_{5\%}$ = 380 N/m and an ultimate strength T_{ult} = 38 kN/m in the machine direction. In the cross-machine direction, the geogrid has a secant stiffness of $J_{5\%}$ = 80 kN/m and an ultimate capacity of T_{ult} = 4 kN/m, both of which are much lower than the values in the machine direciton. Using the similitude relationship in Table 1, the tensile stiffness of the uniaxial geogrid in the machine direction yields a value of 1520 kN/m for the prototype geogrid,

which is in the typical range for uniaxial geogrids used in field structures.

Facing elements for GRS bridge abutments vary with the particular application, and reinforcement-facing connections also change with the type of facing. To meet the similitude relationships, concrete modular facing blocks from Keystone, Inc., with dimensions of 0.3 m × 0.25 m × 0.15 m were selected. A layer of geogrid reinforcement was sandwiched between each course of blocks and connected using fiberglass pins through the geogrid apertures.

Construction

A 0.15 m-thick foundation sand layer was first placed within the edge containment of the shaking table and at a higher relative density (D_r = 85%) than the backfill sand in order to provide a firm base for the GRS bridge abutment. The table surface has transverse shear fins to transfer motion to the foundation layer with minimal slippage. The first course of facing blocks was placed and leveled on the foundation layer, with the side wall blocks offset vertically by 25 mm from the front wall blocks. This offset was needed to avoid direct contact between longitudinal and transverse geogrid layers and maintain interaction with the backfill soil. Although not used in actual GRS bridge abutments, this technique was necessary for the current study due to width constraints of the shaking table. As a result of the 25 mm offset, the side wall and front wall facing blocks could not be interlocked in a typical masonry pattern at the corners.

Longitudinal and transverse reinforcement layers were placed horizontally within the backfill soil from the block contact interfaces and are shown in Figures 5(a) and 5(b), respectively. The transverse reinforcement would not be expected to significantly affect abutment behavior in the longitudinal direction because geogrid stiffness in the cross-machine direction is much lower than in the machine direction; however, the effect of transverse reinforcement should still be included when using results from this test for numerical model validation. During construction, geogrids were placed between the blocks for over 80% of the block-to-block contact surface and the blocks were aligned using fiberglass pins. Although typically grouted together in the field (Helwany et al. 2012), the upper course of blocks remained ungrouted for this test. After construction of the lower GRS wall, the bridge seat was placed on top of the backfill soil for the lower wall and the 0.6 m-high upper wall was constructed in four lifts with only transverse reinforcement layers (Figure 2b). Finally, the concrete bridge beam with additional dead weights was placed on the bridge seat and support wall. A bridge beam is

typically placed prior to construction of upper wall in the field; however, the beam was added last in the current study for convenience.

Values of relative density for the compacted backfill sand, as measured by sand cone, range from 54% to 68%, with an average of 64%. The measured gravimetric water content profile for the backfill sand is shown in Figure 6(a) and indicates values ranging from 3.2% to 6.3%. Considering that the compaction curve is relatively flat for this sand, the variation in water content is unlikely to significantly affect compacted dry unit weight. The gravimetric water content profile can be combined with the SWRC to estimate the apparent cohesion c_a using the suction stress concept of Lu et al. (2010):

$$c_a = \sigma^s \tan\phi' = S_e \psi \tan\phi' \quad (2)$$

where σ^s = suction stress, ψ = matric suction, and S_e = effective saturation, defined as:

$$S_e = \frac{\theta - \theta_{res}}{\theta_{\max} - \theta_{res}} \quad (3)$$

Matric suction values interpreted from the SWRC range from 3 to 10 kPa and yield the calculated profiles of apparent cohesion for drying and wetting conditions shown in Figure 6(b). Apparent cohesion is essentially uniform at approximately 2 kPa for both conditions. Apparent cohesion can have an important effect on the ultimate state of GRS walls (Vahedifard et al. 2014, 2015), and unsaturated conditions can have a significant effect on the stiffness of sand (Khosravi et al. 2010).

INSTRUMENTATION AND INPUT MOTIONS

Instrumentation

Specimen data was collected using an automatic data acquisition system with 160 channels and a simultaneous sampling rate of 256 Hz during shaking. Sensors include string potentiometers (Model P-5A/15A/25A/30A/40A Rayelco, PATRIOT Sensors and Controls Corp.), linear potentiometers (Model 606, BEI sensors), accelerometers (Model CXL02LF1, Crossbow), total pressure cells (Model SPT-3K/6K, AFB Engineered Test System), load cells (Model 1220BF-50K, Interface Inc.), and geogrid strain gauges (KFG-2-120-C1-11, Kyowa Americas, Inc.).

Instrumentation for the longitudinal centerline section (distance from the west side wall

facing y_w = 0.8 m) and transverse section under the bridge seat (distance from front wall facing x = 0.48 m) are shown in Figure 7. Horizontal displacements for the front wall facing blocks at different elevations, bridge seat, reaction wall, bridge beam, and support wall in the longitudinal direction were measured using string potentiometers, and horizontal displacements of the side wall facing blocks were measured using linear potentiometers. Horizontal displacements of the front wall facing for an off-centerline section in the longitudinal direction were also measured (not discussed in this paper). String potentiometers were used to measure settlements at the four corners of the bridge seat. String potentiometers were mounted on rigid reference frames apart from the shaking table and had sufficient tension to measure dynamic motions for the frequency band of the test. The string potentiometer measurements were corrected using measured horizontal displacements of the shaking table in the longitudinal direction to yield relative displacements with respect to the table. Accelerometers were attached on the wall facing and placed within the reinforced and retained soil zones to measure horizontal accelerations in the longitudinal direction. Earth pressure cells were seated into 38 mm-thick PVC plates with plan dimensions of 127 mm × 203 mm for horizontal orientation and 203 mm × 203 mm for vertical orientation. The PVC plates provide a flush surface to improve measurements of vertical and horizontal total stresses. Two load cells were embedded in the south end of the bridge beam to measure potential contact forces between the bridge beam and bridge seat during shaking. Geogrid tensile strains were measured using strain gauges mounted in pairs at the mid-point of longitudinal ribs, with one gauge on top and the other on bottom to correct for rib bending (Runser et al. 2001; Bathurst et al. 2002). Considering that strain gauge measurements may be affected by attachment technique and non-uniform stiffness along a rib (Bathurst et al. 2002), tensile tests were conducted to obtain a correction factor (CF), defined as the ratio of global strain to gauge strain. Calibration results for loading rates of 1%/min, 10%/min, and 100%/min are shown in Figure 8. The data indicate that CF has an average value of 1.1 and is not significantly affected by loading rate. All measured geogrid strains were corrected using this CF value. Within the GRS bridge abutment specimen, strains were measured at 4 points along each of 5 geogrid layers.

Input Motions

A series of motions, including white noise, earthquake, and sinusoidal, were applied to

the GRS bridge abutment system in the longitudinal direction. The shaking table was operated in acceleration-control mode for white noise motions and displacement-control mode for earthquake and sinusoidal motions. A summary of the first five input motions, alternating between white noise and earthquake, is presented in Table 3.

White noise motions were used to characterize natural frequencies of the bridge system, and identify any changes in system response (i.e., modulus and damping) due to strains incurred from previous shaking. The nominal white noise motion has a peak acceleration of 0.1*g*, a root-mean-square (RMS) acceleration of 0.025*g*, and frequency content ranging from 0.1 to 50 Hz. Shaking tests were conducted using motions scaled from the strike-slip 1940 Imperial Valley earthquake (El Centro station) and the subduction zone 2010 Maule earthquake (Concepcion station) records. Acceleration and displacement time histories for the original Imperial Valley record are shown in Figure 9, and indicate a PGA of 0.31*g* and peak ground displacement (PGD) of 130.4 mm. To obtain the input acceleration time history for the shaking test, also shown in Figure 9(a), acceleration amplitudes of the original record were not scaled and frequencies were scaled (increased) by a factor of $\sqrt{2}$ (Table 1). The scaled displacement time history is shown in Fig. 9(b) and was obtained by double integration of the scaled acceleration time history. The displacement motion indicates PGD = 65.2 mm, which is one-half of the PGD for the original record. Scaled input motions for the Maule earthquake record were obtained similarly and yield PGA = 0.40*g* and PGD = 108 mm. The time increments for the scaled Imperial Valley and Maule input motions are 0.00707 s and 0.00354 s, respectively.

RESULTS

Test results, including testing system performance, bridge system identification, facing displacements, bridge seat and bridge beam displacements, acceleration response, and reinforcement strains, during the application of a series of white noise and earthquake input motions in the longitudinal direction are presented. Reported values correspond to model scale, and should be adjusted using the similitude relationships in Table 1 to obtain values for the prototype structures. Horizontal displacements and accelerations in the north direction (Figures 2 and 7), and outward displacements of wall facings are taken as positive. This paper focuses primarily on deformations and acceleration response of the GRS bridge abutment to the two scaled earthquake motions.

Testing System Performance

Measured displacement time histories for the shaking table, reaction wall, and support wall, are shown in Figure 10(a) for the Imperial Valley motion and essentially are in identical agreement with the target input motion. This indicates that (1) the shaking table performed well in displacement-control mode for earthquake motions; (2) the reaction wall is sufficiently stiff and moved essentially in phase with the shaking table; and (3) the steel connection beams and sliding platform successfully transmitted table motions to the base of the support wall. The corresponding measured acceleration time history for the shaking table, shown in Fig. 10(b), contains some high frequency noise but generally matches well with the target input acceleration. The measured PGA of the table is 0.42*g* at 1.6 s, which is larger than the target value of 0.31*g*. A comparison of the response spectra (5% damping) for the shaking table and target input motions is shown in Figure 10(c). The measured pseudo-spectral accelerations for the shaking table agree well with the target values except for some deviations at frequencies between 6 Hz and 9 Hz. This indicates that the shaking table accurately reproduced the salient characteristics of the target motion.

Bridge System Identification

System identification tests were conducted using the white noise motions at different stages of the shaking program. The first such test was conducted on the reaction wall itself prior to construction of the GRS bridge abutment. Amplitudes of the horizontal acceleration transfer functions (i.e., output divided by input in frequency domain) of the reaction wall with respect to the shaking table are shown in Figure 11(a). The reaction wall has a fundamental frequency of 37.5 Hz, which is well above the operating frequency band of the shaking table and fundamental frequency of the GRS bridge abutment. Therefore, the reaction wall is not expected to resonate during shaking and should move essentially in phase with the shaking table, which is consistent with Figure 10(a).

White noise tests also were conducted before and after each earthquake motion to detect changes in fundamental frequency for the bridge system. Horizontal acceleration transfer functions for the bridge beam and bridge seat with respect to the shaking table in the longitudinal direction for the initial white noise test (Shaking event 1) are shown in Figure 11(b). The results

indicate fundamental frequencies of 5.5 Hz and 11.9 Hz for the bridge beam and bridge seat, respectively. Horizontal acceleration transfer functions for the backfill soil with respect to the shaking table, measured at x = 0.48 m, z = 1.875 m inside the GRS bridge abutment, for white noise tests before and after the earthquake motions are shown in Figure 11(c). The GRS bridge abutment has the same fundamental frequency as the bridge seat (11.9 Hz) before the Imperial Valley motion. After the Imperial Valley motion, the fundamental frequency of the abutment decreased from 11.9 to 11.3 Hz, and then decreased further to 10.9 Hz after the Maule motion. These decreases are attributed to shear modulus reduction for the backfill soil during successive shaking events.

Facing Displacements

Time history plots of incremental facing displacements in the longitudinal direction for the front wall facing blocks at selected locations along the centerline section are shown in Figure 12(a) for the Imperial Valley motion. Maximum (i.e., during shaking) and residual (i.e., after shaking) displacements at the top generally are larger than at the bottom. The maximum displacement at elevation z = 1.875 m is 3.7 mm (t = 1.6 s) and the residual displacement is 0.9 mm. For z = 0.075 m, the bottom of the wall had dynamic displacements of ±1 mm.

Profiles of incremental maximum and residual outward facing displacements of the front wall in the longitudinal direction for the Imperial Valley and Maule motions are shown in Figure 12(b). During shaking, maximum displacements for the Maule motion are larger than for the Imperial Valley motion, with values of 4.9 and 3.7 mm at the top of the wall, respectively. These displacement profiles correspond to the specific times associated with maximum displacement measurements (i.e., t = 1.6 s for Imperial Valley and t = 18.0 s for Maule). Fig. 12(b) also shows that the incremental residual displacement profiles are similar for the two earthquake motions. Residual values range from 0.2 to 1.4 mm and generally increase toward the top of the wall. Visual comparison of the maximum and residual profiles clearly indicates that dynamic facing displacements are largely recovered after shaking, especially for the upper sections of the wall. Outward displacement profiles for the west side wall facing in the transverse direction are shown in Figure 12(c) and indicate similar trends. The maximum and residual displacement profiles are similar for the two earthquake motions and increase almost linearly with increasing elevation, with a maximum displacement of 4 mm and residual displacements less than 1 mm.

Figure 12(c) also indicates that shaking in the longitudinal direction induces facing displacements in the transverse direction for the side walls, which is attributed to a Poisson effect associated with bridge seat settlement as discussed in the next section.

Bridge Seat and Bridge Beam Displacements

Settlements of the bridge seat were measured at the four corners (Fig. 2a) and the corresponding incremental time histories for the Maule earthquake motion are presented in Figure 13(a). The bridge seat tilted toward the west during shaking, which is consistent with an initial larger settlement on the same (west) side observed during bridge load application. Average bridge seat settlements for the Maule motion, taken as the average of the four measurements at each time, are shown in Figure 13(b). During shaking, the maximum value is 7.0 mm and the minimum value is -0.2 mm (i.e., uplift). The average residual settlement is 1.4 mm, which corresponds to a vertical strain of 0.07% for the 2.1 m-high lower GRS wall. Average incremental bridge seat settlements for both earthquake motions are summarized in Table 4. For the Imperial Valley motion, the bridge seat had maximum and minimum dynamic settlements of 3.1 mm and -0.1 mm, respectively. The residual settlements were 1.4 mm for both motions, which corresponds to 2.8 mm at prototype scale. Such settlement likely would not be a significant concern for most bridge structures.

Horizontal displacements were measured in the longitudinal direction for the bridge beam and for the bridge seat at the two locations shown in Figure 2(c). Corresponding displacement time histories for the Maule motion are presented in Figure 14. Displacements at the east and west sides of the bridge seat are shown in Figure 14(a) and are similar with respect to both trend and magnitude. This indicates essentially uniform translational movement of the bridge seat in the longitudinal direction during shaking. Maximum and minimum dynamic displacements of the bridge seat are 5.9 and -5.1 mm, respectively. Figure 14(b) indicates that the bridge beam experienced larger dynamic displacements with maximum and minimum values of 13.1 mm and -13.5 mm, respectively. Figure 14(c) presents differential displacements of the bridge beam relative to the bridge seat and indicates a range of approximately ±10 mm and essentially no residual after shaking. These relative displacements are smaller than the initial width of the seismic joint (25 mm), so joint closure and beam-seat contact did not occur during shaking. Final inspection revealed significant slide marks on both sides of the elastomeric bearing pad, which

suggests that relative displacements between the bridge beam and bridge seat occurred primarily as a result of sliding on the pad and not shear deformation of the pad itself.

Acceleration Response

Time histories of horizontal acceleration in the longitudinal direction for the support wall, bridge seat, and bridge beam during the Imperial Valley motion are shown in Figure 15. As in Figure 10(a), the acceleration response of the support wall closely followed the acceleration of the shaking table, which confirms the successful synchronization of the two ends of the bridge system; however, the motion of the support wall also included some additional high frequency response. The bridge seat had a peak acceleration of 0.63*g*, while the bridge beam had a smaller peak acceleration of 0.53*g* and contained less high frequency response. This is attributed to the isolation effect of the elastomeric bearing pad between the bridge seat and bridge beam.

Horizontal acceleration time histories at selected elevations within the reinforced soil zone under the bridge seat (x = 0.48 m in Figure 2b) are shown for the Imperial Valley motion in Figure 16(a). Similar to the facing displacements in Figure 12(a), soil accelerations increase with elevation and thus indicate increasing amplification toward the top of the GRS bridge abutment. The RMS method can be used to mitigate effects of high frequency noise and also characterize amplitude and frequency content in a measured response (Kramer 1996; El-Emam and Bathurst 2005). Figure 16(b) shows the profile of RMS acceleration ratio within the reinforced soil zone (x = 0.48 m) for the Imperial Valley motion, where the RMS acceleration at each location is normalized by the shaking table RMS acceleration. Acceleration ratio increases essentially linearly with elevation for the three sections and again indicates increasing amplification toward the top of the abutment. Maximum acceleration ratios were measured at the highest elevation (z = 1.875 m), and are equal to 1.56, 1.57, and 1.59 for the retained soil zone, reinforced soil zone, and front wall facing, respectively.

Reinforcement Strains

Reinforcement tensile strains in the longitudinal direction at three elevations under the bridge seat (x = 0.45 m) are shown in Figure 17 for the Imperial Valley motion. All strain values remained positive (i.e., tensile) during the test. Measured strains for the top and bottom strain gauges are in close agreement at z = 0.075 and z = 0.975 m, and show a similar trend but

different magnitudes at z = 1.875 m. This indicates bending of the geogrid at z = 1.875 m during construction and highlights the importance of installing top and bottom gauges at each strain measurement location. Maximum dynamic reinforcement strains in the middle geogrid layer are higher than in the upper and lower geogrid layers for this test.

Distributions of tensile strain along five reinforcement layers at different elevations within the longitudinal section are shown in Figure 18(a) for the Imperial Valley motion. Each measurement represents the average from a pair of top and bottom gauges and corresponds to an initial (before shaking), maximum (during shaking), minimum (during shaking), or residual (after shaking) value. Zero strain at the free end of each reinforcement layer is also plotted. The distributions of initial reinforcement strain show peak values near the facing connection (x = 0.10 m) for lower layers 1, 4, and 7, and under the bridge seat (x = 0.45 m) for upper layers 10 and 13. Similar to data reported by Runser et al. (2001) for a tall retaining wall with steel strip reinforcements, initial strains at the connections increase and then decrease with depth after construction. During shaking, maximum strains also are highest near the connections for lower layers and under the bridge seat for upper layers, whereas minimum strains generally are close to the initial values. The maximum dynamic values indicate increased strains near the connections, which is attributed to inertial forces of the facing blocks. Except for the bottom reinforcement layer, residual strains near the connections increased only slightly as compared to initial values and indicate that the majority of dynamic reinforcement strains were recovered at the facing. Residual strains under the bridge seat increased significantly, especially for upper reinforcement layers.

Strain distributions along three reinforcement layers in the transverse section are shown in Figure 18(b) for the Imperial Valley motion. Similar to reinforcement in the longitudinal section, high initial and residual strains occur near the connections for layers 1 and 7, and under the bridge seat for layer 13. During shaking, minimum strains are close to the initial values and maximum strains are close to the residual values. Thus, dynamic strains generally were not recovered after shaking for the transverse reinforcement. As a result, for example, the strain in layer 13 under the bridge seat (y_w = 0.33 m) increased approximately 0.1% due to shaking, which is substantially higher than the corresponding increase of approximately 0.04% (x = 0.45 m) at the same elevation in the longitudinal direction. The data of Figure 18(b) indicate that shaking caused significant increases in strain for the transverse reinforcement, which suggests

that, in addition to longitudinal reinforcement analysis, analysis of transverse reinforcement is important for seismic design.

SUMMARY AND CONCLUSIONS

This paper presents an experimental study of the dynamic response of a half-scale GRS bridge abutment system using a shaking table. Experimental design of the model specimen followed established similitude relationships for shaking table tests of reduced-scale models in a 1*g* gravitational field, including scaling of model geometry, geosynthetic reinforcement stiffness, backfill soil modulus, bridge load, and characteristics of the earthquake motions. The 2.7 m-high GRS bridge abutment was constructed using well-graded sand backfill, modular facing blocks, and uniaxial geogrid reinforcement with a vertical spacing of 0.15 m in both the longitudinal and transverse directions. The GRS bridge abutment model corresponds to a prototype GRS bridge abutment with a total height of 5.4 m and a bridge clearance height of 4.5 m. A bridge beam was placed on the GRS bridge abutment at one end and on a concrete support wall resting on a sliding platform off the shaking table at the other end. The bottom of the concrete support wall was rigidly connected to the shaking table using steel beams to transmit horizontal table motions. The bridge system was subjected to a series of input motions in the longitudinal direction, including white noise motions for system identification and scaled motions from the 1940 Imperial Valley and 2010 Maule earthquakes.

Experimental results indicate that the shaking table performed well in displacement-control mode and the steel connection beams and sliding platform successfully transmitted motions from the table to the base of the support wall. Results also indicate that the GRS bridge abutment experienced small deformations. After each of the Imperial Valley and Maule motions, incremental residual facing displacements in model scale were as large as 1.0 mm for both the longitudinal and transverse sections, and incremental residual bridge seat settlements in model scale were 1.4 mm, which yields a vertical strain of 0.7% for the GRS bridge abutment. The acceleration ratio for the wall facing and within the backfill soil increased essentially linearly with elevation, indicating progressive motion amplification toward the top of the abutment. Residual strains in the geogrid reinforcements increased slightly near the facing connections and increased significantly under the bridge seat in the longitudinal direction due to dynamic loading. The increase of residual reinforcement strains in the upper layer in the transverse section is

substantially higher than the corresponding increase at the same elevation in the longitudinal direction, which indicates that the analysis of transverse reinforcements is important for seismic design of these structures.

It is important to acknowledge that the testing program and results presented in this study are limited by the size and payload capacity of the shaking table. In particular, GRS bridge abutments in the field have a much larger retained soil mass behind the reinforced soil zone, which may increase wall facing displacements, abutment settlement, and reinforcement strains. Also, the width of the GRS bridge abutment model in this study is smaller than a proportionally-scaled GRS bridge abutment in the field, which likely changes the 3D aspects of the dynamic response. In particular, the small width the GRS bridge abutment model required overlap of geogrid reinforcements in the transverse and longitudinal directions and may have produced an overall stiffer response than a scaled GRS bridge abutment in the field where such an overlap would be limited to the regions near the side walls. Nonetheless, results of this study provide valuable insights into the seismic behavior of GRS bridge abutments and experimental data that can be used for calibration of numerical models.

ACKNOWLEDGMENTS

Financial support for this study was provided by the California Department of Transportation (Caltrans) and Federal Highway Administration (FHWA) Pooled Fund Project 65A0556, and is gratefully acknowledged. The authors thank Dr. Charles Sikorsky of the Caltrans Office of Earthquake Engineering for his support and assistance with the project. The authors also thank the staff and undergraduate research assistants at the UCSD Powell Structural Laboratories for their help with the experimental work. In addition, we would like to thank Tony Allen, State Geotechnical Engineer from the Washington Department of Transportation (WSDOT), Kathryn Griswell from Caltrans, and Willie Liew, Chief Engineer, from Tensar International Corporation, for their assistance. We also thank Dr. Richard Bathurst of the Royal Military College of Canada for several helpful discussions regarding details of the experimental program.

REFERENCES

Adams, M., Nicks, J., Stabile, T., Wu, J., Schlatter, W., and Hartmann, J., 2011, "Geosynthetic Reinforced Soil Integrated Bridge System Interim Implementation Guide," *FHWA-HRT-11-026*, U.S. DOT, Washington, D.C.

ASTM D6637-15: Standard Test Method for Determining Tensile Properties of Geogrids by the Single or Multi-Rib Tensile Method, ASTM International, West Conshohocken, PA, 2015.

Bathurst, R. J., Allen, T. M., and Walters, D. L., 2002, "Short-Term Strain and Deformation Behavior of Geosynthetic Walls at Working Stress Conditions," *Geosynthetics International*, Vol. 9, Nos. 5-6, pp. 451-482.

Casey, J. A., Soon, D., Kutter, B., and Romstad, K., 1991, "Modeling of Mechanically Stabilized Earth Systems: A Seismic Centrifuge Study," *Geotechnical Engineering Congress*, Vol. II, ASCE, Reston, VA, pp. 839-850.

El-Emam, M. M., and Bathurst, R. J., 2004, "Experimental Design, Instrumentation and Interpretation of Reinforced Soil Wall Response using a Shaking Table," *International Journal of Physical Modelling in Geotechnics*, Vol. 4, No. 4, pp. 13-32.

El-Emam, M. M., and Bathurst, R. J., 2005, "Facing Contribution to Seismic Response of Reduced-Scale Reinforced Soil Walls," *Geosynthetics International*, Vol. 12, No. 5, pp. 215-238.

El-Emam, M. M., and Bathurst, R. J., 2007, "Influence of Reinforcement Parameters on the Seismic Response of Reduced-Scale Reinforced Soil Retaining Walls," *Geotextiles and Geomembranes*, Vol. 25, No. 1, pp. 33-49.

Fox, P. J., Andrew, A. C., Elgamal, A., Greco, P., Isaacs, D., Stone, M., and Wong, S., 2015, "Large Soil Confinement Box for Seismic Performance Testing of Geo-Structures," *Geotechnical Testing Journal*, Vol. 38, No. 1, pp. 72-84.

Fox, P. J., Rowland, M. G., Scheithe, J. R., Davis, K. L., Supple, M. R., and Crow, C. C., 1997, "Design and Evaluation of a Large Direct Shear Machine for Geosynthetic Clay Liners," *Geotechnical Testing Journal*, Vol. 20, No. 3, pp. 279-288.

Fox, P. J., Nye, C. J., Morrison, T. C., Hunter, J. G., and Olsta, J. T., 2006, "Large Dynamic Direct Shear Machine for Geosynthetic Clay Liners," *Geotechnical Testing Journal*, Vol. 29, No. 5, pp. 392-400.

Guler, E., and Enunlu, A. K., 2009, "Investigation of Dynamic Behavior of Geosynthetic Reinforced Soil Retaining Structures under Earthquake Loads," *Bulletin of Earthquake Engineering*, Vol. 7, No. 3, pp. 737-777.

Guler, E., and Selek, O, 2014, "Reduced-scale Shaking Table Tests on Geosynthetic-Reinforced Soil Walls with Modular Facing," *Journal of Geotechnical and Geoenvironmental Engineering*, 10.1061/(ASCE)GT.1943-5606.0001102, 04014015.

Helwany, S. M. B., Wu, J. T. H., and Kitsabunnarat, A., 2007, "Simulating the Behavior of GRS Bridge Abutments," *Journal of Geotechnical and Geoenvironmental Engineering*, Vol. 133, No. 10, pp. 1229-1240.

Helwany, S. M. B., Wu, J. T. H., and Meinholz, P., 2012, "Seismic Design of Geosynthetic-reinforced Soil Bridge Abutments with Modular Block Facing," *NCHRP Web-Only Document 187*, Transportation Research Board, Washington, D.C.

Howard, R. W. A., Kutter, B. L., and Siddharthan, R., 1998, "Seismic Deformation of Reinforced Soil Centrifuge Models," *Geotechnical Earthquake Engineering and Soil Dynamics III*, ASCE, Reston, VA, pp. 446-468.

Iai, S., 1989, "Similitude for Shaking Table Tests on Soil-Structure-Fluid Models in 1g Gravitational Fields," *Soils and Foundations*, Vol. 29, No. 1, pp. 105-118.

Khosravi, A., Ghayoomi, M., McCartney, J. S., and Ko, H.-Y., 2010, "Impact of Effective Stress on the Dynamic Shear Modulus of Unsaturated Sands," *GeoFlorida 2010: Advances in Analysis, Modeling & Design*, Orlando, FL, 410-419.

Koseki, J., Munaf, Y., Tatsuoka, F., Tateyama, M., Kojima, K., and Sato, T., 1998, "Shaking and Tilt Table Tests of Geosynthetic-Reinforced Soil and Conventional-Type Retaining Walls," *Geosynthetics International*, Vol. 5, Nos. 1-2, pp. 73-96.

Kramer, S. L., *Geotechnical Earthquake Engineering*, Prentice Hall, Upper Saddle River, NJ, 1996, 653pp.

Krishna, A. M., and Latha, G. M., 2009, "Seismic Behavior of Rigid-Faced Reinforced Soil Retaining Wall Models: Reinforcement Effect," *Geosynthetics International*, Vol. 16, No. 5, pp. 364-373.

Latha, G. M., and Krishna, A. M., 2008, "Seismic Response of Reinforced Soil Retaining Wall Models: Influence of Backfill Relative Density," *Geotextiles and Geomembranes*, Vol. 26, No. 4, pp. 335-349.

Latha, G. M., and Santhanakumar, P., 2015, "Seismic Response of Reduced-Scale Modular Block and Rigid Faced Reinforced Walls through Shaking Table Tests," *Geotextiles and Geomembranes*, Vol. 43, No. 4, pp. 307-316.

Ling, H. I., Leshchinsky, D., Wang, J., Mohri, Y., and Rosen, A., 2009, "Seismic Response of Geocell Retaining Walls: Experimental Studies," *Journal of Geotechnical and Geoenvironmental Engineering*, Vol. 135, No. 4, pp. 515-524.

Ling, H. I., Leshchinsky, D., Mohri, Y., and Wang, J., 2012, "Earthquake Response of Reinforced Segmental Retaining Walls Backfilled with Substantial Percentage of Fines," *Journal of Geotechnical and Geoenvironmental Engineering,* Vol. 138, No. 8, pp. 934-944.

Ling, H. I., Mohri, Y., Leshchinsky, D., Burke, C., Matsushima, K., and Liu, H., 2005, "Large-Scale Shaking Table Tests on Modular Block Reinforced Soil Retaining Walls," *Journal of Geotechnical and Geoenvironmental Engineering*, Vol.131, No. 4, pp. 465-476.

Liu, H., Wang, X., and Song, E., 2010, "Centrifuge Testing of Segmental Geosynthetic-Reinforced Soil Retaining Walls subjected to Modest Seismic Loading," *GeoFlorida 2010*, *Advances in Analysis, Modeling and Design*, ASCE, Reston, VA, pp. 2992-2998.

Lu, N., Godt, J. W., and Wu, D. T., 2010, "A Closed-form Equation for Effective Stress in Unsaturated Soil," *Water Resources Research*, Vol. 46, W05515, 10.1029/2009WR008646.

Matsuo, O., Tsutsumi, T., Yokoyama, K., and Saito, Y., 1998, "Shaking Table Tests and Analyses of Geosynthetic-Reinforced Soil Retaining Walls," *Geosynthetics International*, Vol. 5, Nos. 1-2, pp. 97-126.

Nicks, J. E., Adams, M. T., Ooi, P. S. K., and Stabile, T., 2013, "Geosynthetic Reinforced Soil Performance Testing – Axial Load Deformation Relationships," *FHWA-HRT-13-066*, U.S. DOT, Washington, D.C.

Nicks, J. E., Esmaili, D., and Adams, M. T., 2016, "Deformations of Geosynthetic Reinforced Soil under Bridge Service Loads," *Geotextiles and Geomembranes*, Vol. 44, No. 4, pp. 641-653.

Nova-Roessig, L., and Sitar, N., 2006, "Centrifuge Model Studies of the Seismic Response of Reinforced Soil Slopes," *Journal of Geotechnical and Geoenvironmental Engineering*, Vol. 132, No. 3, pp. 388-400.

Panah, A. K., Yazdi, M., and Ghalandarzadeh, A., 2015, "Shaking Table Tests on Soil Retaining Walls Reinforced by Polymeric Strips," *Geotextiles and Geomembranes*, Vol. 43, No. 2, pp. 148-161.

Richardson, G. N., and Lee, K. L., 1975, "Seismic Design of Reinforced Earth Walls," *Journal of the Geotechnical Engineering Division*, Vol. 10, No. 12, pp. 167-188.

Runser, D., Fox, P. J., and Bourdeau, P. L., 2001, "Field Performance of a 17 m-high Reinforced Soil Retaining Wall." *Geosynthetics International*, Vol. 8, No. 5, pp. 367-391.

Sabermahani, M., Ghalandarzadeh, A., and Fakher, A., 2009, "Experimental Study on Seismic Deformation Modes of Reinforced-soil Walls," *Geotextiles and Geomembranes*, Vol. 27, No. 2, pp. 121-136.

Sakaguchi, M., 1996, "A Study of the Seismic Behavior of Geosynthetic Reinforced Walls in Japan," *Geosynthetics International*, Vol. 3, No. 1, pp. 13-30.

Siddharthan, R. V., Ganeshwara, V., Kutter, B. L., El-Desouky, M., and Whitman, R. V., 2004, "Seismic Deformation of Bar Mat Mechanically Stabilized Earth Walls. I: Centrifuge Tests," *Journal of Geotechnical and Geoenvironmental Engineering*, Vol. 130, No. 1, pp. 14-25.

Trautner, C. A., Zheng, Y., McCartney, J. S., and Hutchinson, T. C., 2017, "An Approach for Shake Table Performance Evaluation during Repair and Retrofit Actions," *Earthquake Engineering and Structural Dynamics* (in review).

Vahedifard, F., Leshchinsky, B., Sehat, S., and Leshchinsky, D., 2014, "Impact of Cohesion on Seismic Design of Geosynthetic-Reinforced Earth Structures," *Journal of Geotechnical and Geoenvironmental Engineering*, 10.1061/(ASCE)GT.1943-5606.0001099, 04014016.

Vahedifard, F., Leshchinsky, B., Mortezaei, K., and Lu, N., 2015, "Active Earth Pressures for Unsaturated Retaining Structures," *Journal of Geotechnical and Geoenvironmental Engineering*, 10.1061/(ASCE)GT.1943-5606.0001356, 04015048.

van Genuchten, M.T., 1980, "A Closed-Form Equation for Predicting the Hydraulic Conductivity of Unsaturated Soils," *Soil Science Society of America Journal*, Vol. 44, No. 5, pp. 892–898.

Wu, J. T. H., Ketchart, K., and Adams, M., 2001, "GRS Bridge Piers and Abutments," *Report No. FHWA-RD-00-038*, U.S. DOT, Washington, D.C.

Wu, J. T. H., Lee, K. Z. Z., Helwany, S. B., and Ketchart, K., 2006, "Design and Construction Guidelines for Geosynthetic-Reinforced Soil Bridge Abutments with a Flexible Facing," *NCHRP Report 556*, Transportation Research Board, Washington, D.C.

Zheng, Y., and Fox, P. J., 2016, "Numerical Investigation of Geosynthetic-Reinforced Soil Bridge Abutments under Static Loading," *Journal of Geotechnical and Geoenvironmental Engineering*, 10.1061/(ASCE)GT.1943-5606.0001452, 04016004.

Zheng, Y., and Fox, P. J., 2017, "Numerical Investigation of the Geosynthetic Reinforced Soil-Integrated Bridge System under Static Loading," *Journal of Geotechnical and Geoenvironmental Engineering*, 10.1061/(ASCE)GT.1943-5606.0001665, 04017008.

TABLE AND FIGURE CAPTIONS

TABLE 1 Similitude relationships for 1*g* shaking table tests (Iai 1989).

TABLE 2 Backfill soil properties.

TABLE 3 Input motions for shaking table.

TABLE 4 Average incremental bridge seat settlements for two earthquake motions.

FIG. 1 Shaking table test configuration for bridge system in the longitudinal direction.

FIG. 2 GRS bridge abutment model: (a) top view; (b) longitudinal cross-sectional view; (c) transverse cross-sectional view. Note: dashed lines indicate reinforcement layers perpendicular to diagram.

FIG. 3 Bridge support wall: (a) end view; (b) low-friction sliding platform.

FIG. 4 Backfill soil properties: (a) particle size gradation curve; (b) standard Proctor compaction curve.

FIG. 5 Construction of GRS bridge abutment: (a) longitudinal reinforcement layer; (b) transverse reinforcement layer.

FIG. 6 Soil profile information for GRS bridge abutment: (a) gravimetric water content; (b) calculated apparent cohesion.

FIG. 7 Instrumentation: (a) longitudinal section (y_w = 0.8 m); (b) transverse section (x = 0.48 m).

FIG. 8 Calibration relationship for strain gauge measurements.

FIG. 9 Original records and scaled motions for the 1940 Imperial Valley earthquake (El Centro station): (a) acceleration time history; (b) displacement time history.

FIG. 10 Imperial Valley motion: (a) displacement time history; (b) acceleration time history; (c) response spectra (5% damping).

FIG. 11 Horizontal acceleration transfer function amplitudes from white noise tests: (a) reaction wall only; (b) bridge seat and bridge beam with respect to shaking table for initial white noise motion (Shaking event 1); (c) GRS bridge abutment (x = 0.48 m, z = 1.875 m) before and after two earthquake motions (Shaking events 1, 3, 5).

FIG. 12 Facing displacements: (a) time histories for front wall in longitudinal section for the Imperial Valley motion; (b) profiles for front wall in longitudinal section; (c) profiles for side wall in transverse section (note: sensor at z = 1.575 m non-responsive).

FIG. 13 Time histories of bridge seat settlement for the Maule motion: (a) four corner measurements; (b) average values.

FIG. 14 Time histories of horizontal displacement in the longitudinal direction for the Maule motion: (a) bridge seat; (b) bridge beam; (c) bridge beam relative to bridge seat.

FIG. 15 Time histories of horizontal acceleration for the Imperial Valley motion: (a) support wall; (b) bridge seat; (c) bridge beam.

FIG. 16 Horizontal acceleration response for the Imperial Valley motion: (a) time histories in reinforced soil zone; (b) RMS acceleration ratio profiles for three sections.

FIG. 17 Time histories of reinforcement tensile strain in the longitudinal direction at three elevations for the Imperial Valley motion.

FIG. 18 Distributions of reinforcement strain for the Imperial Valley motion: (a) longitudinal section; (b) transverse section.

TABLE 1 Similitude relationships for 1*g* shaking table tests (Iai 1989).

Variable	Theoretical scaling factor	Scaling factor for $\lambda = 2$
Length	λ	2
Material density	1	1
Strain	1	1
Mass	λ^3	8
Acceleration	1	1
Velocity	$\lambda^{1/2}$	1.414
Stress	λ	2
Modulus	λ	2
Stiffness	λ^2	4
Force	λ^3	8
Time	$\lambda^{1/2}$	1.414
Frequency	$\lambda^{-1/2}$	0.707

TABLE 2 Backfill soil properties.

Property	Value
Specific gravity, G_s	2.61
Coefficient of uniformity, C_u	6.1
Coefficient of curvature, C_z	1.0
Maximum void ratio, e_{max}	0.853
Minimum void ratio, e_{min}	0.371
Peak friction angle, $\phi_p^{'}$ (°)	51.3
van Genuchten (1980) SWRC model parameter, α_{vG} (kPa^{-1})	0.5
van Genuchten (1980) SWRC model parameter, N_{vG}	2.1
Drying curve volumetric water content at zero suction, θ_d (m^3/m^3)	0.32
Wetting curve volumetric water content at zero suction, θ_w (m^3/m^3)	0.20
Residual volumetric water content, θ_r (m^3/m^3)	0.00

TABLE 3 Input motions for shaking table.

Shaking event	Motion	Model-scale duration (s)	Target PGA (*g*)	Actual PGA (*g*)	Target PGD (mm)	Actual PGD (mm)
1	White noise	60.0	0.10	0.17	2.7	5.6
2	Imperial Valley	28.3	0.31	0.42	65.2	65.2
3	White noise	60.0	0.10	0.16	2.7	5.9
4	Maule	100.4	0.40	0.58	108.0	108.0
5	White noise	60.0	0.10	0.15	2.7	5.8

TABLE 4 Average incremental bridge seat settlements for two earthquake motions.

Earthquake motion	Maximum dynamic settlement (mm)	Minimum dynamic settlement (mm)	Residual settlement (mm)
Imperial Valley	3.1	-0.1	1.4
Maule	7.0	-0.2	1.4

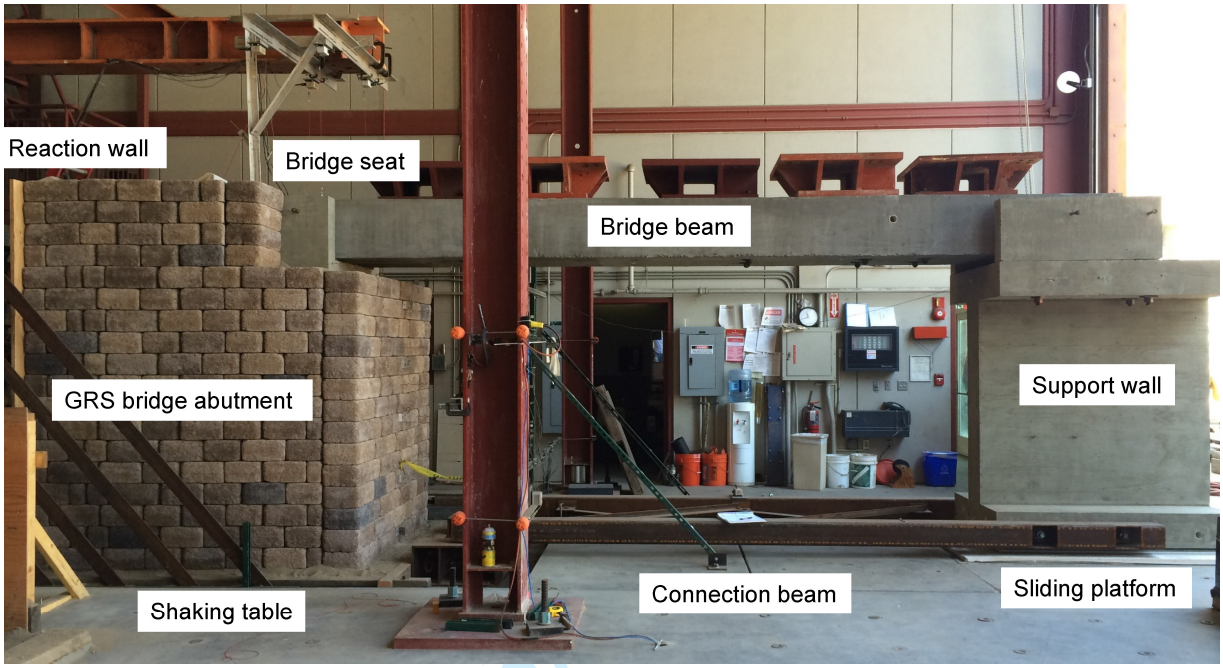

FIG. 1 Shaking table test configuration for bridge system in the longitudinal direction.

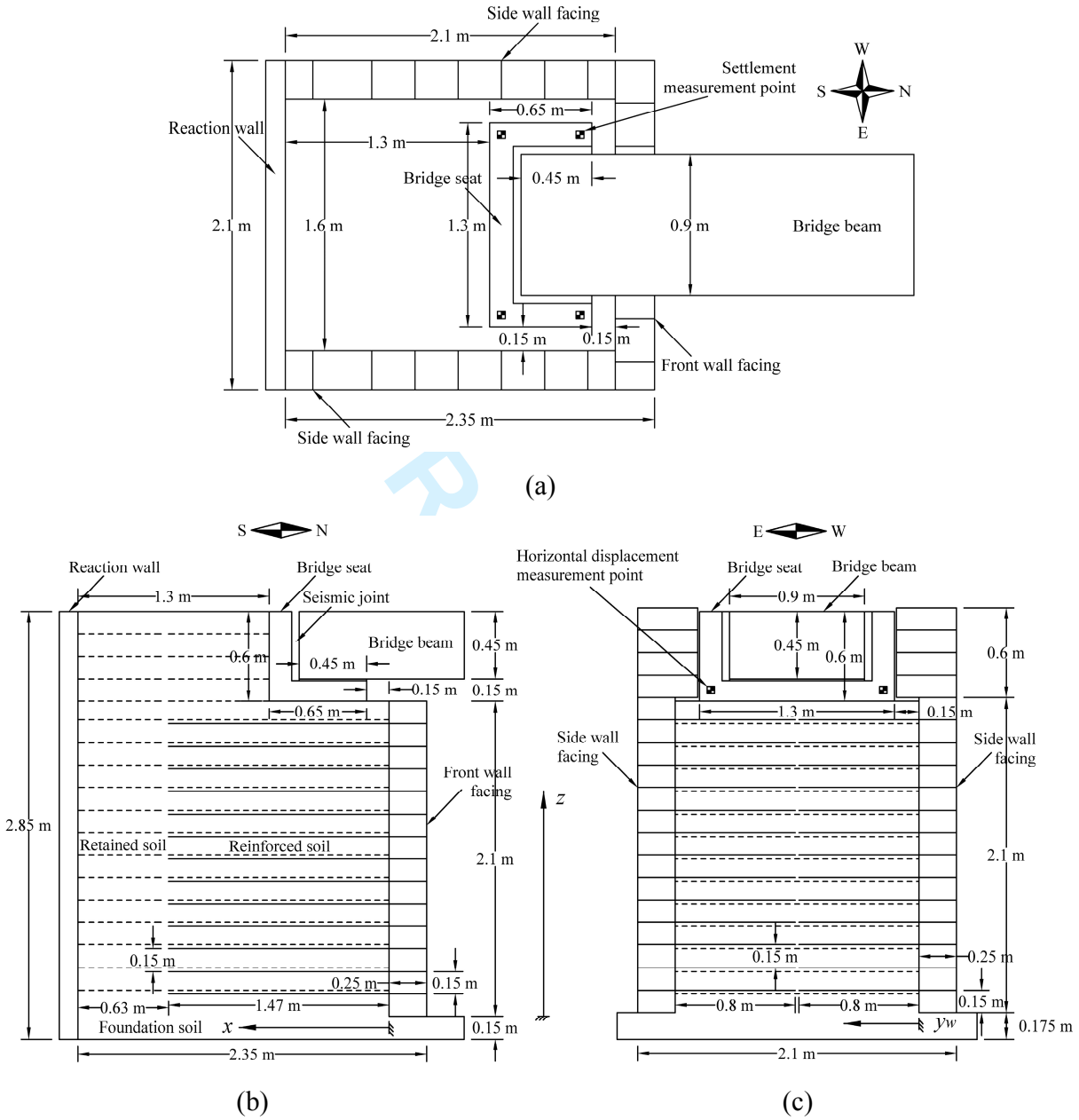

FIG. 2 GRS bridge abutment model: (a) top view; (b) longitudinal cross-sectional view; (c) transverse cross-sectional view. Note: dashed lines indicate reinforcement layers perpendicular to diagram.

(a)

(b)

FIG. 3 Bridge support wall: (a) end view; (b) low-friction sliding platform.

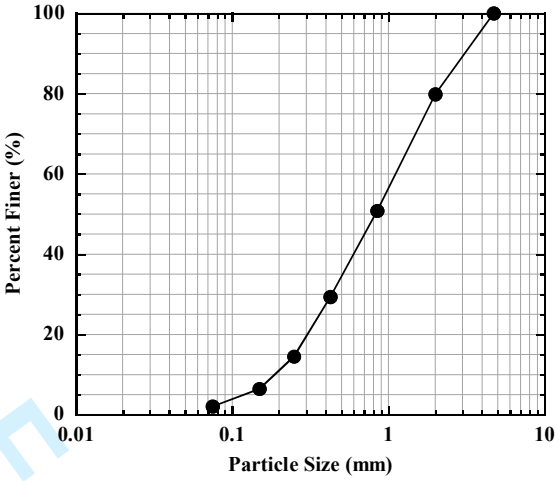

(a)

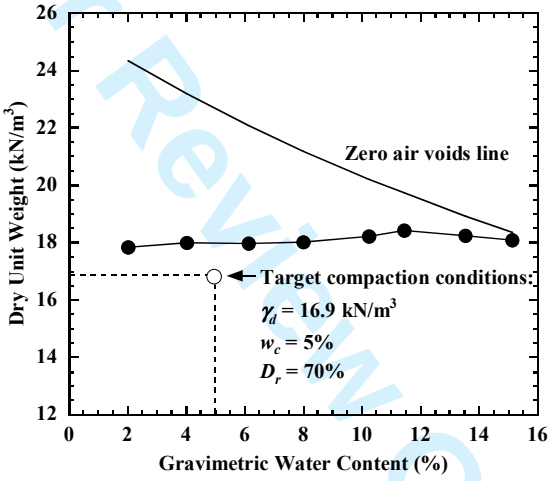

(b)

FIG. 4 Backfill soil properties: (a) particle size gradation curve; (b) standard Proctor compaction curve.

(a) (b)

FIG. 5 Construction of GRS bridge abutment: (a) longitudinal reinforcement layer; (b) transverse reinforcement layer.

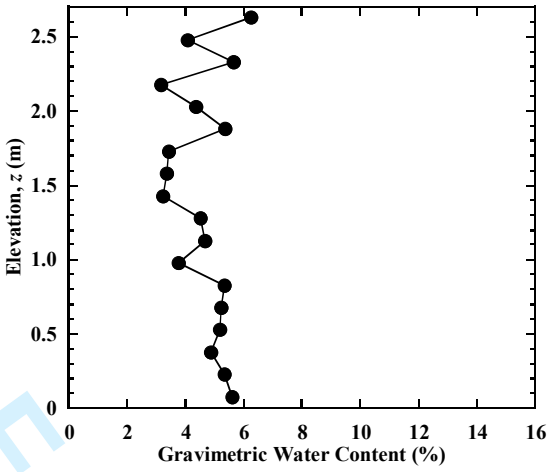

(a)

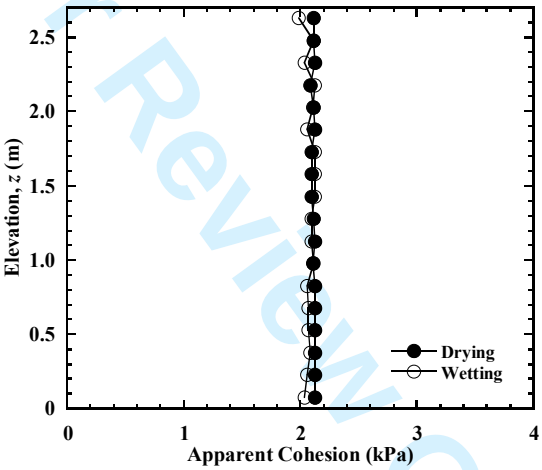

(b)

FIG. 6 Soil profile information for GRS bridge abutment: (a) gravimetric water content; (b) calculated apparent cohesion.

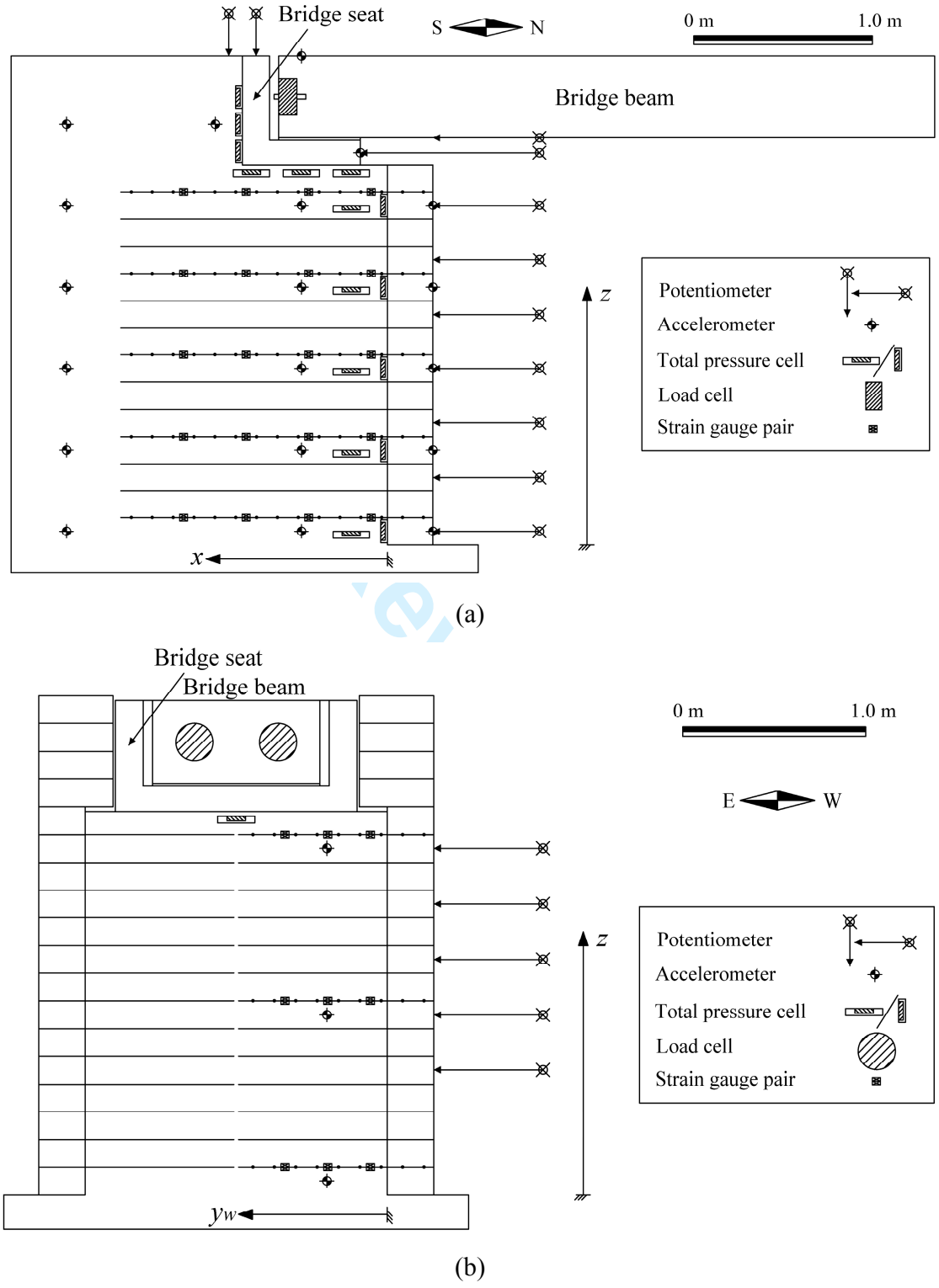

FIG. 7 Instrumentation: (a) longitudinal section (y_w = 0.8 m); (b) transverse section (x = 0.48 m).

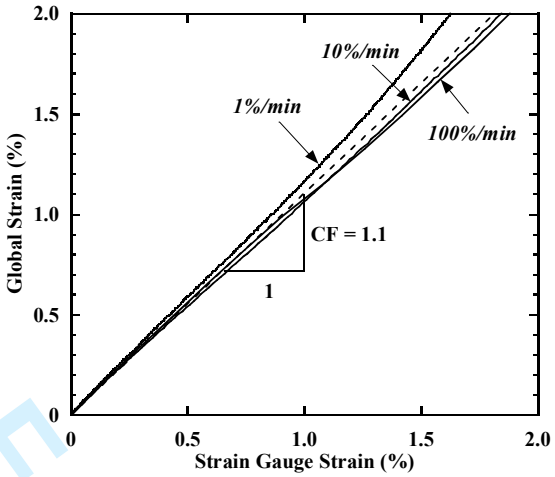

FIG. 8 Calibration relationship for strain gauge measurements.

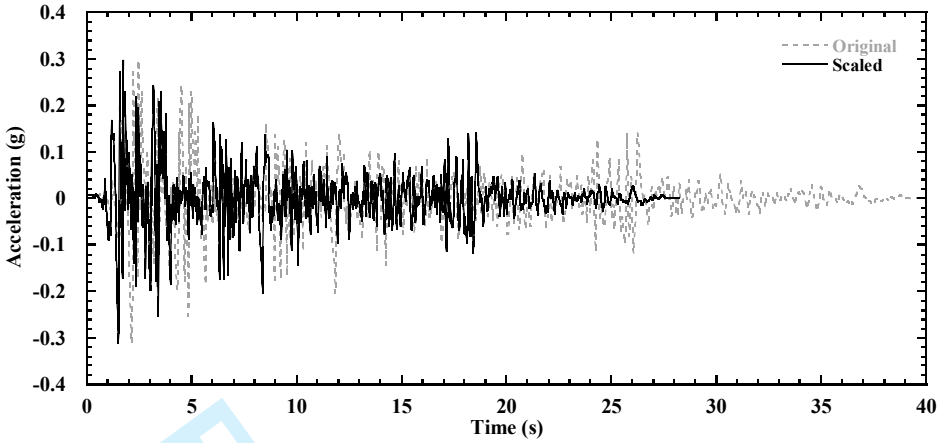

(a)

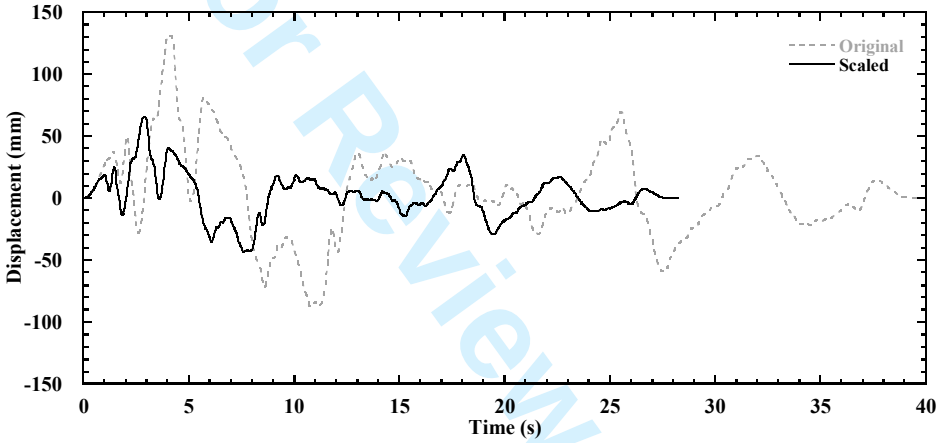

(b)

FIG. 9 Original records and scaled motions for the 1940 Imperial Valley earthquake (El Centro station): (a) acceleration time history; (b) displacement time history.

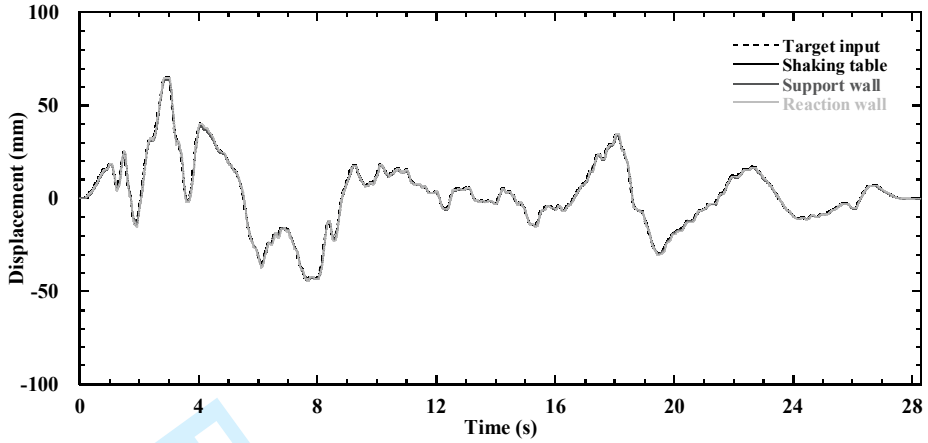

(a)

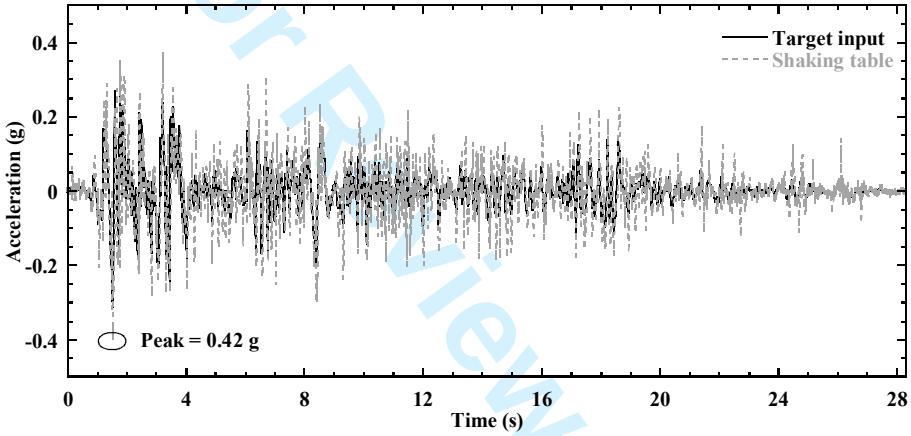

(b)

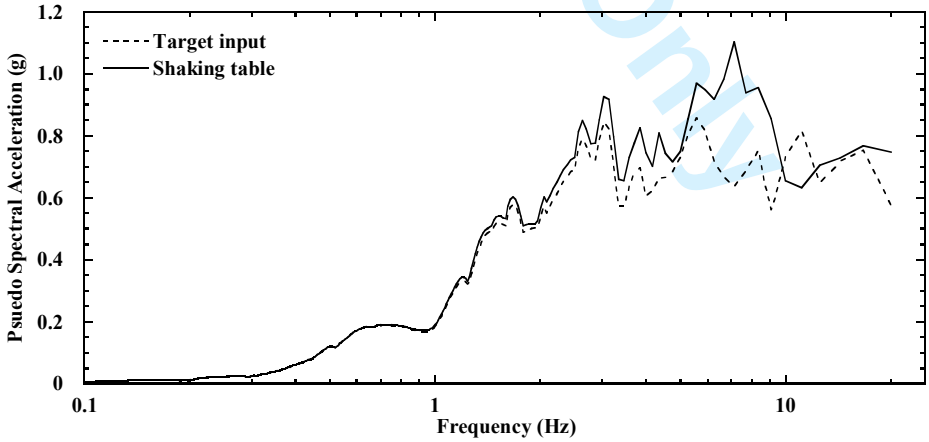

(c)

FIG. 10 Imperial Valley motion: (a) displacement time history; (b) acceleration time history; (c) response spectra (5% damping).

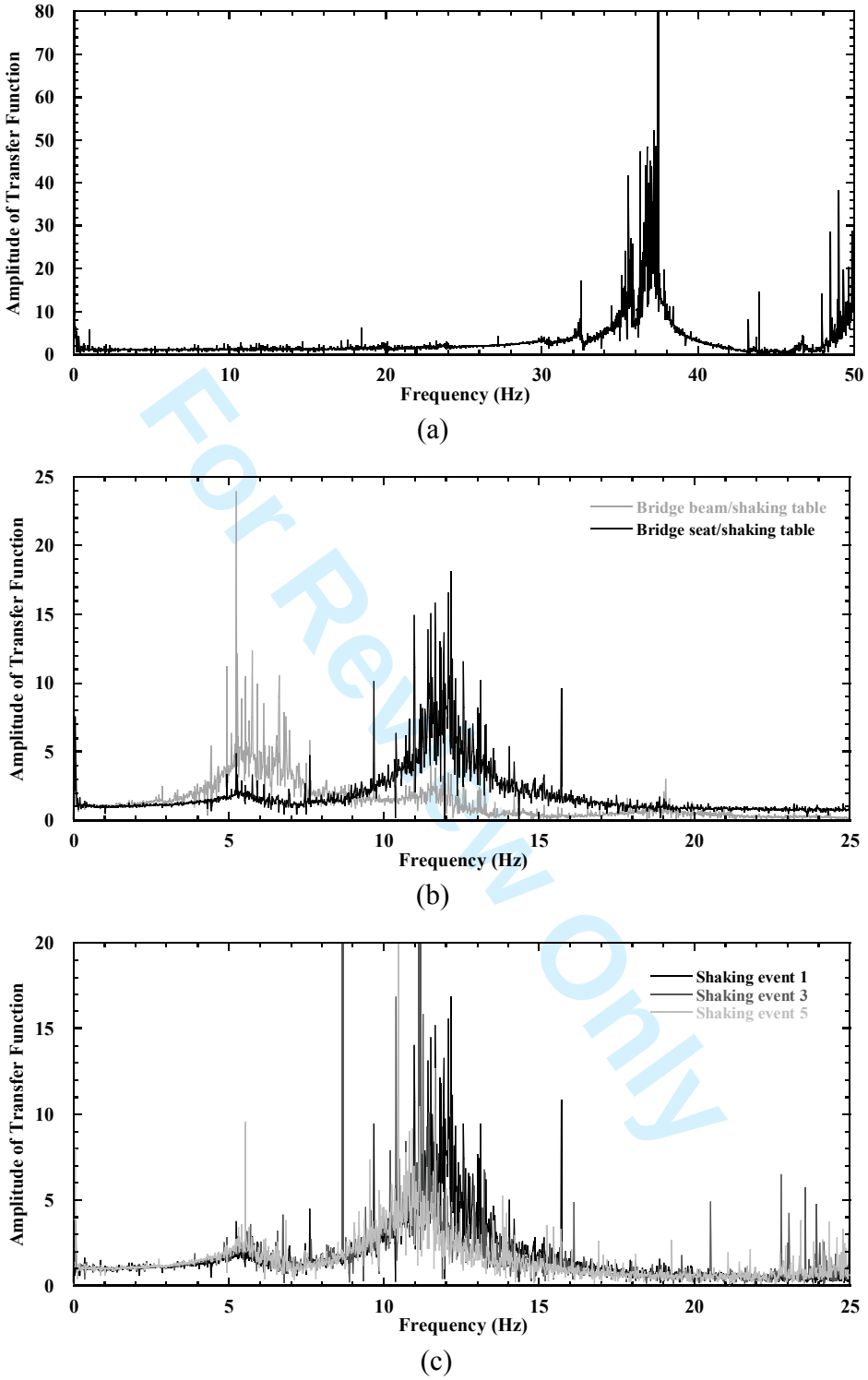

FIG. 11 Horizontal acceleration transfer function amplitudes from white noise tests: (a) reaction wall only; (b) bridge seat and bridge beam with respect to shaking table for initial white noise motion (Shaking event 1); (c) GRS bridge abutment (x = 0.48 m, z = 1.875 m) before and after two earthquake motions (Shaking events 1, 3, 5).

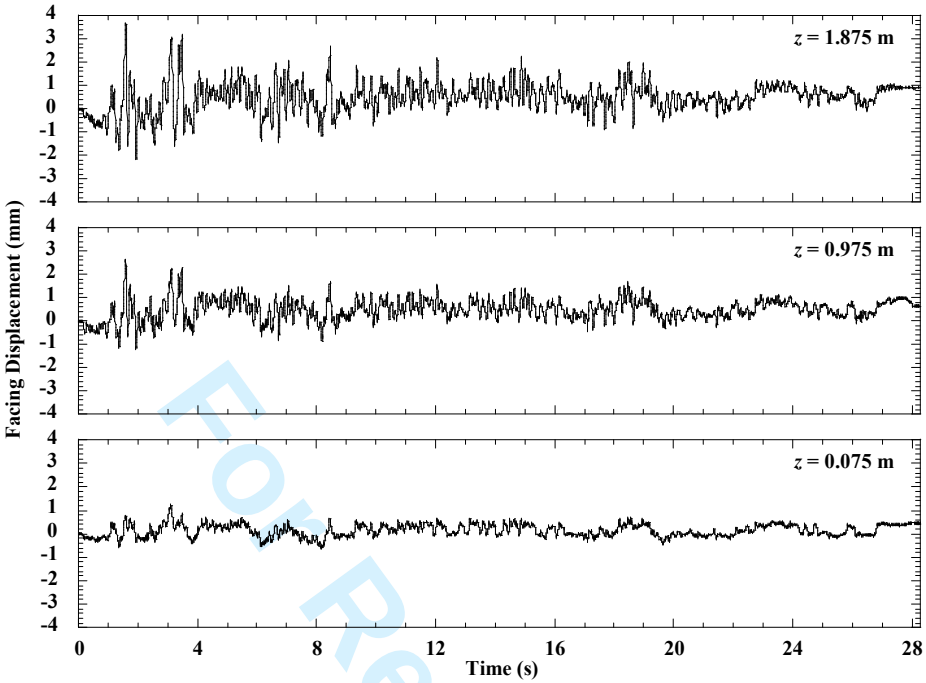

(a)

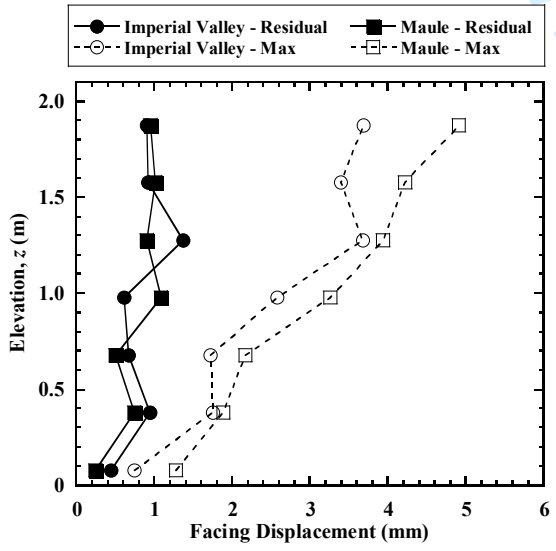

(b)

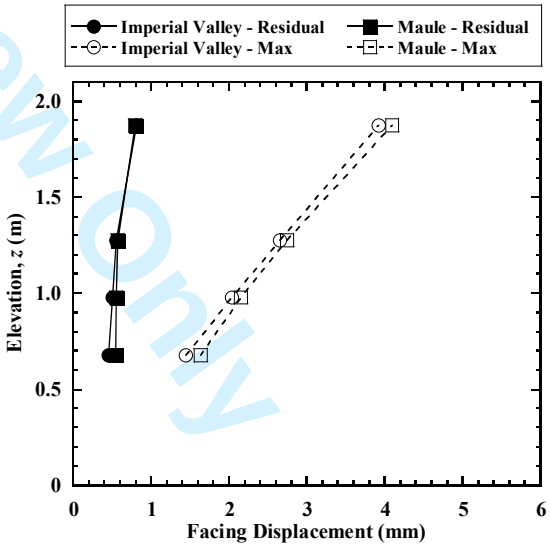

(c)

FIG. 12 Facing displacements: (a) time histories for front wall in longitudinal section for the Imperial Valley motion; (b) profiles for front wall in longitudinal section; (c) profiles for side wall in transverse section (note: sensor at z = 1.575 m non-responsive).

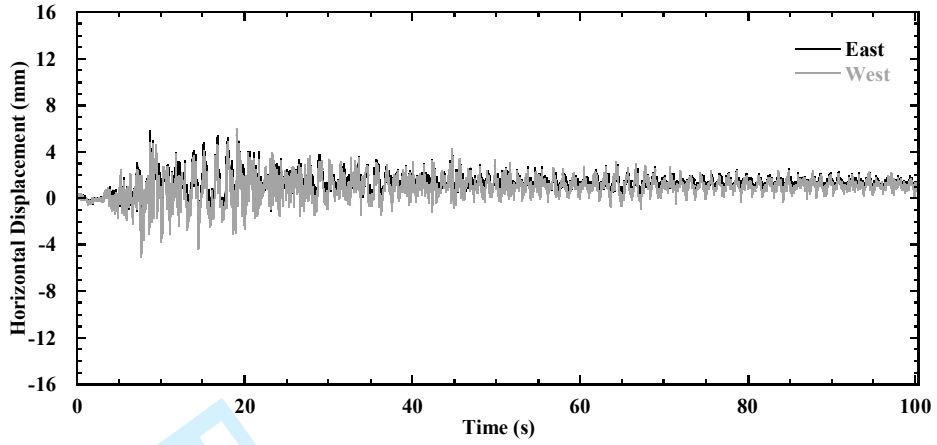

(a)

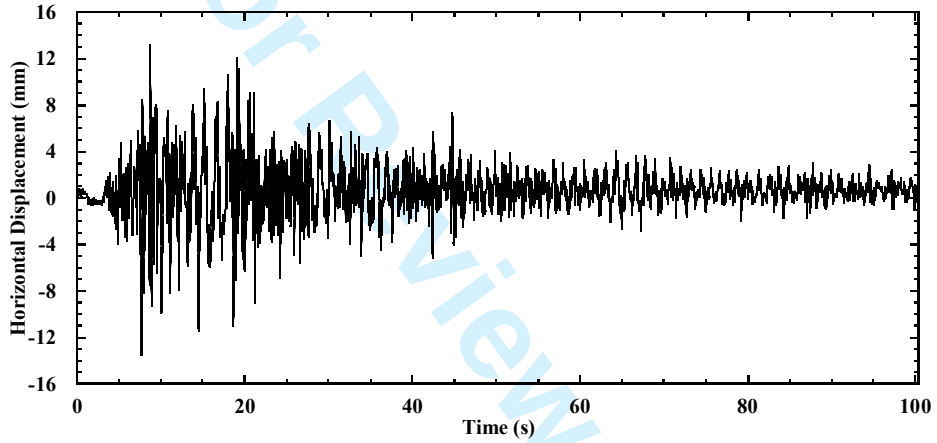

(b)

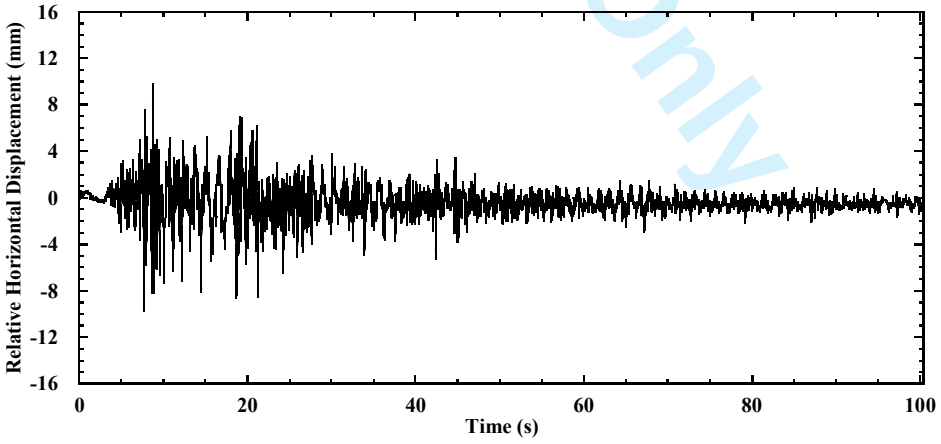

(c)

FIG. 14 Time histories of horizontal displacement in the longitudinal direction for the Maule motion: (a) bridge seat; (b) bridge beam; (c) bridge beam relative to bridge seat.

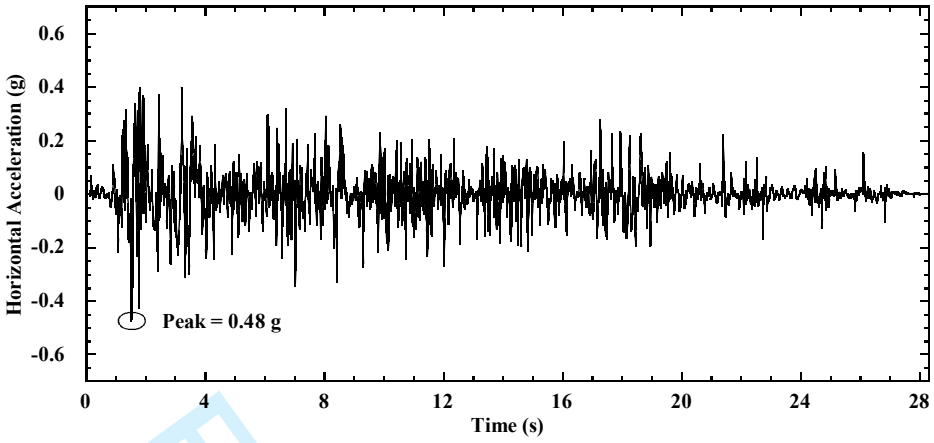

(a)

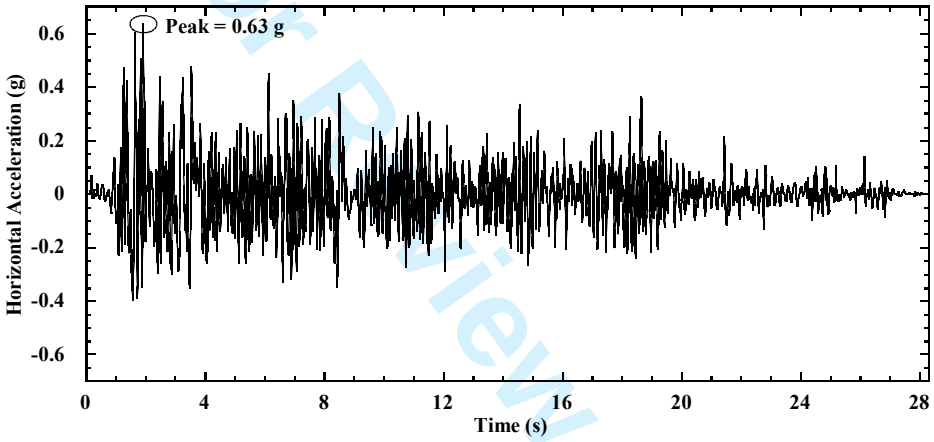

(b)

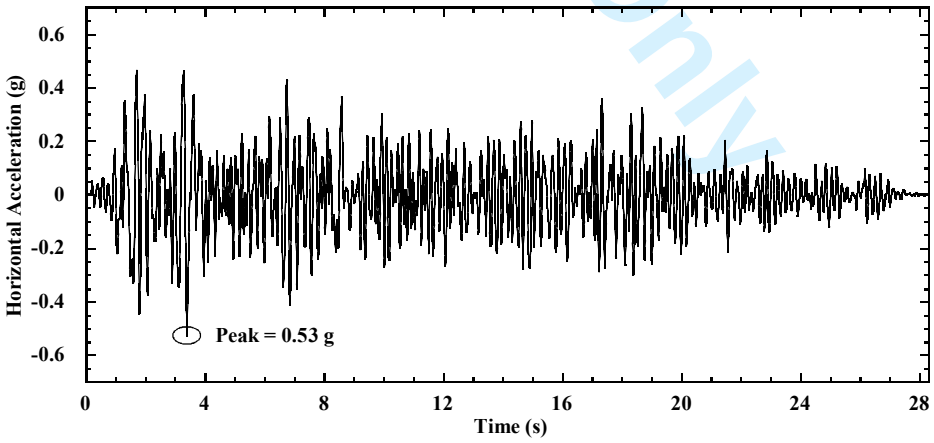

(c)

FIG. 15 Time histories of horizontal acceleration for the Imperial Valley motion: (a) support wall; (b) bridge seat; (c) bridge beam.

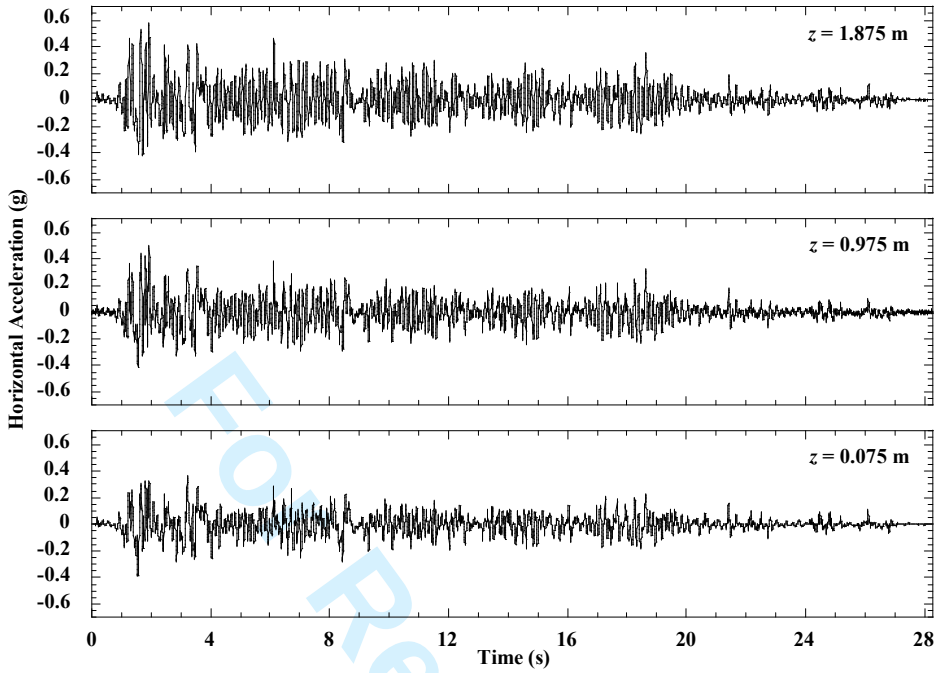

(a)

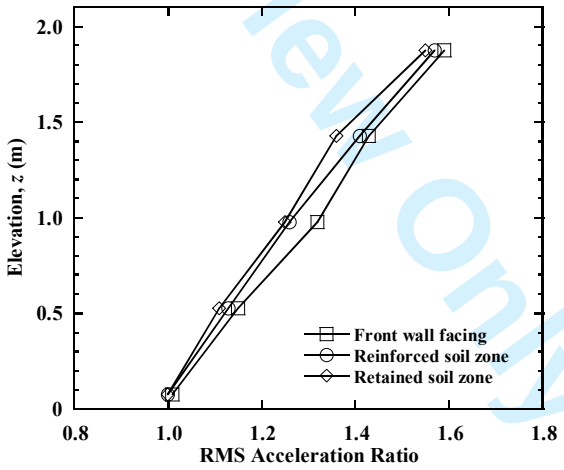

(b)

FIG. 16 Horizontal acceleration response for the Imperial Valley motion: (a) time histories in reinforced soil zone; (b) RMS acceleration ratio profiles for three sections.

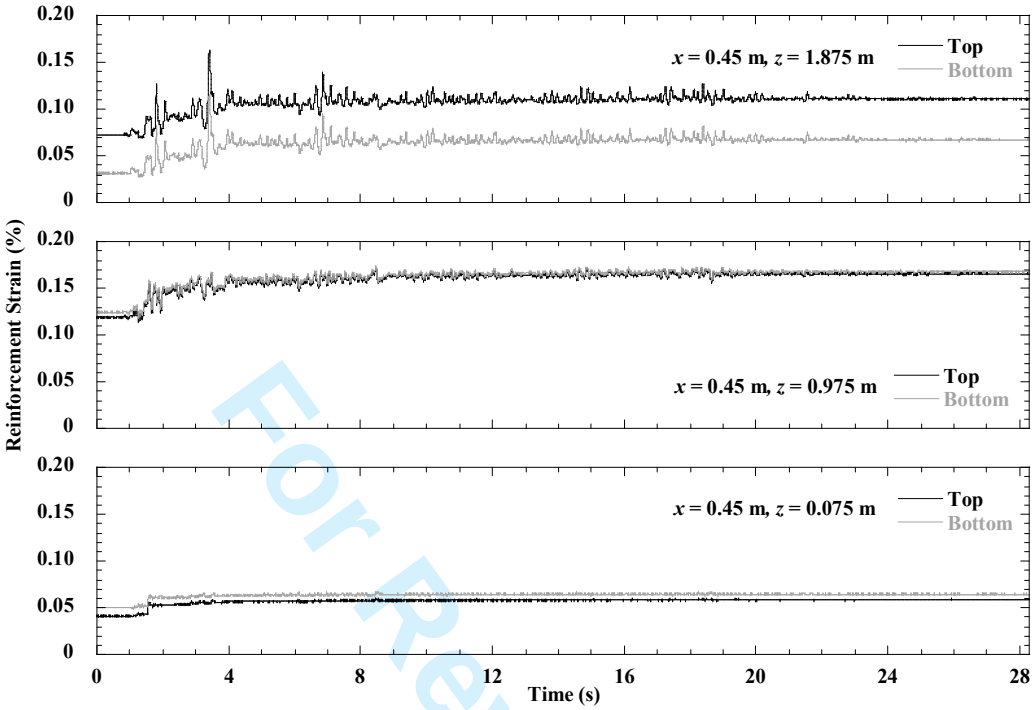

FIG. 17 Time histories of reinforcement tensile strain in the longitudinal direction at three elevations for the Imperial Valley motion.

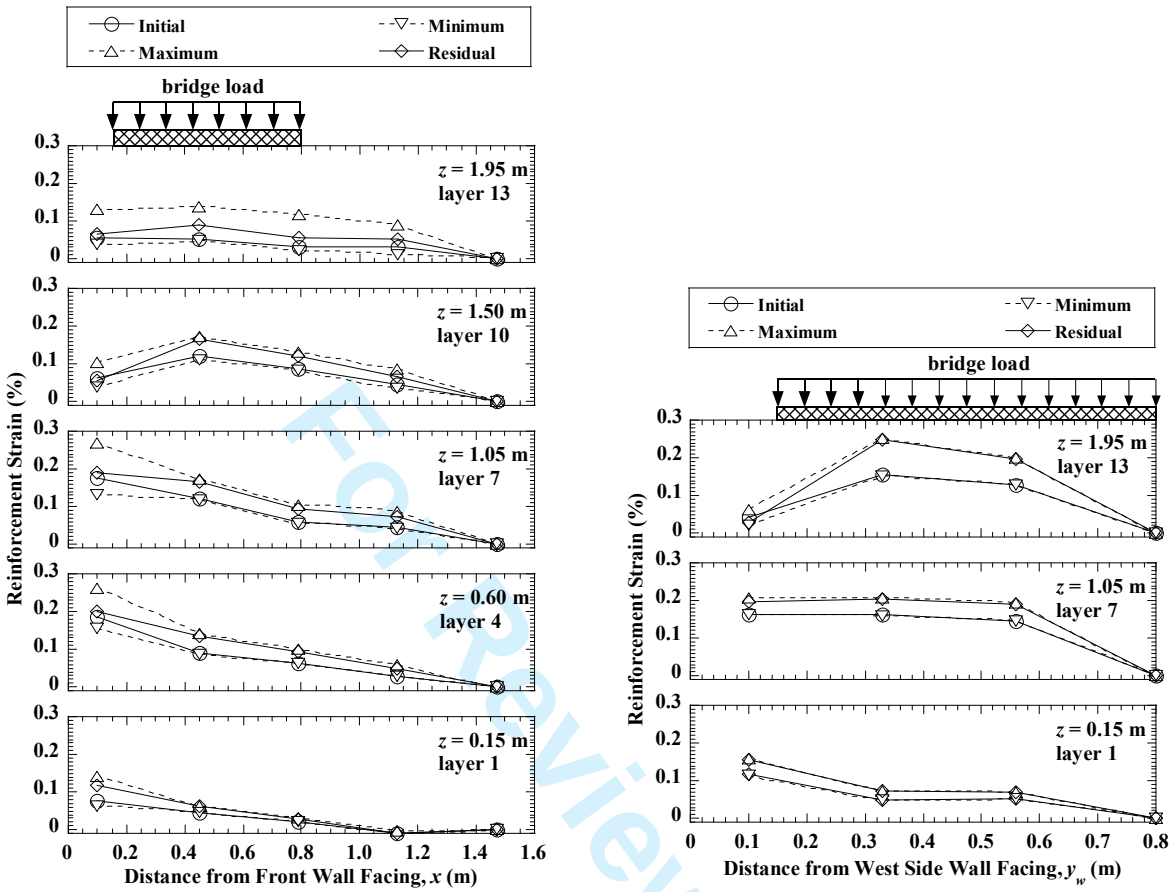

(a) (b)

FIG. 18 Distributions of reinforcement strain for the Imperial Valley motion: (a) longitudinal section; (b) transverse section.